Revisiting step instabilities on crystal surfaces. Part II: General theory

Laurent Guin, Michel E. Jabbour, Leopold Shaabani-Ardali, Nicolas Triantafyllidis

J. Mech. Phys. Solids 156 (2021) 104582

Contents lists available at ScienceDirect

Journal of the Mechanics and Physics of Solids

journal homepage: www.elsevier.com/locate/jmps

Revisiting step instabilities on crystal surfaces. Part II: General theory

L. Guin [*,a,b,c], M.E. Jabbour [a,d], L. Shaabani-Ardali [f,g], N. Triantafyllidis [a,d,e]

[a] LMS, École polytechnique, CNRS, Institut Polytechnique de Paris, Palaiseau 91128, France
[b] LPICM, École polytechnique, CNRS, Institut Polytechnique de Paris, Palaiseau 91128, France
[c] Mechanics & Materials Lab, Department of Mechanical and Process Engineering, ETH Zürich, Zürich 8092, Switzerland
[d] Département de Mécanique, École polytechnique, Palaiseau 91128, France
[e] Departments of Aerospace Engineering & Mechanical Engineering (Emeritus), The University of Michigan, Ann Arbor MI 48109-2140, USA
[f] LadHyX, École polytechnique, CNRS, Institut Polytechnique de Paris, Palaiseau 91128, France
[g] DAAA, ONERA, Université Paris-Saclay, Meudon F-92190, France

ARTICLE INFO

Keywords:
A. crystal growth
A. morphological instability
A. step bunching
C. stability and bifurcation
C. quasistatic approximation

ABSTRACT

The quasistatic approximation is a useful but questionable simplification for analyzing step instabilities during the growth/evaporation of vicinal surfaces. Using this approximation, we characterized in Part I of this work the effect on stability of different mechanisms and their interplay: elastic step-step interactions, the Schwoebel barrier, and the chemical coupling of the diffusion fields on adjacent terraces. In this second part, we present a stability analysis of the general problem without recourse to the quasistatic approximation. This analysis reveals the existence of a supplementary mechanism, which we label the "dynamics effect" as it follows from accounting for all the convective and transient terms in the governing equations. This effect can be stabilizing or destabilizing depending on the ratio of step attachment/detachment kinetics to terrace diffusion kinetics. Further, we find that this dynamics effect remains significant in the slow deposition/evaporation regime, thereby invalidating the classical postulate underlying the quasistatic approximation. Finally, revisiting experiments of crystal growth on Si(111)-7 × 7 and GaAs(001), our analysis provides an alternative explanation of the observed step bunching, one that does not require the mechanisms previously invoked in the literature.

1. Introduction

In Part I of this work, we formulated the problem of growth (including sublimation) by step flow on a vicinal surface and proceeded with the linear stability analysis of its quasistatic approximation. This simplification permitted a mostly analytical treatment of stability, thereby yielding significant insight into the influence of the various elementary mechanisms at play on the onset of step bunching. In Part II, we go beyond the quasistatic approximation by investigating the stability of a vicinal surface with respect to bunching in the framework of the general step-flow problem. Our present analysis unveils a new stabilizing/destabilizing mechanism associated with the dynamical terms neglected in the quasistatic approximation, which we refer to as the "dynamics effect." As we shall establish, this stability analysis furnishes an explanation of the observed step bunching on such semiconductor surfaces as Si(111)-7 × 7 and GaAs(001), one that circumvents the appeal to mechanisms that have been invoked in the literature but whose existence and

* Corresponding author.
E-mail address: laguin@ethz.ch (L. Guin).

https://doi.org/10.1016/j.jmps.2021.104582
Received 22 March 2021; Received in revised form 17 July 2021; Accepted 19 July 2021
Available online 24 July 2021

ubiquity remain debated.

Assuming that the terrace adatom densities remain close to their equilibrium value and that the steps are straight and in thermodynamic equilibrium (so that the configurational force that drives step migration vanishes at each step), the dimensionless moving-boundary problem that captures the evolution of a vicinal surface (by deposition and/or evaporation) in the step-flow regime is given by

$$\begin{cases} \partial_t \rho_n &= \partial_{xx}\rho_n - \overline{\nu}\rho_n + \overline{F}, \\ -\rho_n^- \dot{x}_{n+1} - (\partial_x \rho_n)^- &= \underbrace{\overline{\kappa}\left(\rho_n^- - 1 - \chi\Theta[\![\rho]\!]_{x_{n+1}} + \mathfrak{f}_{n+1}\right)}_{J_{n+1}^-} - \overline{\kappa}_p [\![\rho]\!]_{x_{n+1}}, \\ \rho_n^+ \dot{x}_n + (\partial_x \rho_n)^+ &= \underbrace{\overline{\kappa} S\left(\rho_n^+ - 1 - \chi\Theta[\![\rho]\!]_{x_n} + \mathfrak{f}_n\right)}_{J_n^+} + \overline{\kappa}_p [\![\rho]\!]_{x_n}, \\ \dot{x}_n &= \Theta\left(J_n^+ + J_n^-\right), \\ \mathfrak{f}_n &= \sum_{\substack{r\in\{-R,\dots,R\} \\ r\neq 0}} \left\{ \frac{\overline{\beta}}{x_{n+r} - x_n} - \frac{\overline{\alpha}}{(x_{n+r} - x_n)^3} \right\}, \end{cases} \tag{1}$$

where $\rho_n(x,t)$ is the adatom density on the nth terrace, $x_n(t)$ and $x_{n+1}(t)$ denote the positions of its bounding steps, and $\mathfrak{f}_n$ is the elastic contribution to the configurational force acting of the nth step (cf. Section 2 of Part I for details).

As discussed in Section 2.5 of Part I, the *quasistatic approximation* is obtained by neglecting the transient term $\partial_t\rho_n$ in $(1)_1$, as well as the "convective" terms $\rho_n^-\dot{x}_{n+1}$ in $(1)_2$ and $\rho_n^+\dot{x}_n$ in $(1)_3$, resulting in considerable simplification of the stability analysis. To the best of our knowledge, no previous work has explored the consequences of the inclusion of these dynamical terms on the stability of steps based on the general equations (1). This is the goal of Part II of our study.

In terms of method, the challenge raised by the stability analysis of (1) lies in that both the adatom density functions and their domains of definition are subject to perturbations. To address this issue we use an arbitrary Lagrangian-Eulerian (ALE) mapping of (1), which allows us to formulate the linear stability problem as a periodic system of infinite size, subsequently rewritten on a unit cell (one terrace) by means of the Floquet-wave decomposition. The stability problem hence takes the form of a generalized eigenvalue problem, solved numerically using a Chebyshev collocation method.

That general theory reveals dynamics (a term we use to designate collectively the transient term in the PDE and the "convective" terms in the associated boundary conditions) as a new stabilizing/destabilizing mechanism, which we characterize by isolating it from the other mechanisms discussed in Part I. We find that, both under deposition and evaporation, the effect of dynamics on stability depends on the value of $\overline{\kappa}$ (which expresses the ratio of step attachment/detachment kinetics to terrace diffusion kinetics). When combined with the remaining mechanisms (i.e., elastic step-step interactions, the Ehrlich–Schwoebel barrier, and the chemical effect, which encapsulates the thermodynamically necessary coupling between the diffusion fields on adjacent terraces), dynamics significantly modifies the stability diagrams obtained in Part I in the quasistatic regime. This finding calls for the reinterpretation of some experimental results. In this regard, we show that the general stability analysis provides a novel explanation for the observed onset of step bunching on Si(111)-7 $\times$ 7 and GaAs(001).

The rest of the article is organized as follows. The general stability analysis of (1) is presented in Section 2 and its results are given in Section 3. In Section 4, we reinterpret some experiments in which step bunching is observed. Finally, we return in Section 5 to the quasistatic approximation and discuss how our analysis compares with previous works on dynamics. We summarize our main results in Section 6.

2. Stability analysis including dynamics terms

In this section, we perform the linear stability analysis of the step-flow moving boundary problem (1). Unlike its counterpart in the quasistatic approximation (cf. Section 3 of Part I), which furnishes a closed-form expression for the growth rate of any perturbation, the present analysis, which accounts for the dynamical terms, yields stability results that are numerical. The fundamental steady-state solution is computed in Section 2.1. This is followed in Section 2.2 by the stability analysis, which involves three steps: an arbitrary Lagrangian-Eulerian mapping of (1), the linearization of the resulting equations about the steady-state solution, and a Floquet-wave analysis of the linearized equations. This procedure delivers, for each wavelength of instability, a generalized eigenvalue problem whose numerical resolution gives the growth rate associated with the mode of instability in question.

2.1. Steady-state solution

Like in Section 3.1 of Part I, the fundamental solution of (1) corresponds to the propagation of equidistant steps, with the nth step position given by $\overset{\circ}{x}_n(t) = n + \overset{\circ}{V}t$ and the adatom density $\overset{\circ}{\rho}(x,t)$ expressed as

$$\overset{\circ}{\rho}(x,t) = \widetilde{\overset{\circ}{\rho}}\left(x - \overset{\circ}{x}_n(t)\right), \tag{2}$$

for $x \in (\overset{\circ}{x}_n(t), \overset{\circ}{x}_n(t)+1)$, where $\widetilde{\overset{\circ}{\rho}}$ is defined on (0,1). Substitution of (2) into $(1)_{1,2,3}$ yields an analytical expression for $\widetilde{\overset{\circ}{\rho}}$ in terms of the unknown step velocity $\overset{\circ}{V}$. The subsequent insertion of the resulting currents J_n^- and J_n^+ into $(1)_4$ yields an equation for $\overset{\circ}{V}$. In the deposition regime ($\bar{\nu} = 0$), this equation can be solved analytically and, as it turns out, one recovers the velocity associated with the quasistatic steady-state solution, $\overset{\circ}{V} = \overline{F}\Theta$. By contrast, in the presence of evaporation ($\bar{\nu} \neq 0$), $(1)_4$ yields a transcendental equation for $\overset{\circ}{V}$ which must be solved numerically.

2.2. Linear stability

Arbitrary Lagrangian-Eulerian formulation

We turn to the linear stability of the steady-state solution of (1). To circumvent the difficulty of moving boundaries, we use an Arbitrary Lagrangian-Eulerian (ALE) formulation by which we substitute the ALE variable $u \in (0,1)$ to the spatial variable $x \in (x_n(t), x_{n+1}(t))$ through the change of variable

$$u := \frac{x - x_n(t)}{x_{n+1}(t) - x_n(t)}. \tag{3}$$

We then introduce the ALE adatom density $\widetilde{\rho}_n(u,t)$ on nth terrace, defined on $(0,1)\times\mathbb{R}^+$ by

$$\widetilde{\rho}_n(u,t) := \rho_n\Big(\big[x_{n+1}(t) - x_n(t)\big]u + x_n(t), t\Big), \tag{4}$$

and, letting $s_n(t) := x_{n+1}(t) - x_n(t)$, rewrite (1) as

$$\begin{cases} s_n^2\partial_t\widetilde{\rho}_n &= \partial_{uu}\widetilde{\rho}_n + s_n\Big(\dot{x}_n + \Big(\dot{x}_{n+1} - \dot{x}_n\Big)u\Big)\partial_u\widetilde{\rho}_n + s_n^2\Big(-\overline{\nu}\widetilde{\rho}_n + \overline{F}\Big), \\ -s_n\widetilde{\rho}_n^-\dot{x}_{n+1} - \big(\partial_u\widetilde{\rho}_n\big)^- &= s_n\left(\underbrace{\overline{\kappa}\Big(\widetilde{\rho}_n^- - 1 - \chi\Theta\Big(\widetilde{\rho}_{n+1}^+ - \widetilde{\rho}_n^-\Big) + \mathfrak{f}_{n+1}\Big)}_{\widetilde{J}_{n+1}^-} - \overline{\kappa}_p\Big(\widetilde{\rho}_{n+1}^+ - \widetilde{\rho}_n^-\Big)\right), \\ s_n\widetilde{\rho}_n^+\dot{x}_n + \big(\partial_u\widetilde{\rho}_n\big)^+ &= s_n\left(\underbrace{\overline{\kappa}S\Big(\widetilde{\rho}_n^+ - 1 - \chi\Theta\Big(\widetilde{\rho}_n^+ - \widetilde{\rho}_{n-1}^-\Big) + \mathfrak{f}_n\Big)}_{\widetilde{J}_n^+} + \overline{\kappa}_p\Big(\widetilde{\rho}_n^+ - \widetilde{\rho}_{n-1}^-\Big)\right), \\ \dot{x}_n &= \Theta\Big(\widetilde{J}_n^+ + \widetilde{J}_n^-\Big), \end{cases} \tag{5}$$

where $\widetilde{\rho}_n^+(t) := \widetilde{\rho}_n(0,t)$, $\widetilde{\rho}_n^-(t) := \widetilde{\rho}_n(1,t)$, $(\partial_u\widetilde{\rho}_n)^+(t) := \partial_u\widetilde{\rho}_n(0,t)$ and $(\partial_u\widetilde{\rho}_n)^-(t) := \partial_u\widetilde{\rho}_n(1,t)$.

Linear perturbation equations

Noting that for the steady-state solution $u = x - \overset{\circ}{x}_n(t)$, the ALE form of the principal solution is $\widetilde{\overset{\circ}{\rho}}(u)$, with $\widetilde{\overset{\circ}{\rho}}$ obtained in Section 2.1. The linear-perturbation equations are obtained by perturbing step positions and adatom densities:

$$\begin{cases} x_n(t) &= n + \overset{\circ}{V}t + \varepsilon\delta x_n(t), \\ \widetilde{\rho}_n(u,t) &= \widetilde{\overset{\circ}{\rho}}(u) + \varepsilon\delta\widetilde{\rho}_n(u,t), \end{cases} \tag{6}$$

where ε is a small parameter. Restricting attention to nearest-neighbor elastic interactions between steps, i.e., taking $R = 1$ in $(1)_4$,[1] inserting (6) in (5), and collecting terms of order ε yields a linear system for $\mathbf{q}_n(u,t) := (\delta x_n(t), \delta\widetilde{\rho}_n(u,t))$,

$$\mathscr{A}(\mathbf{q}_{n-1}, \mathbf{q}_n, \mathbf{q}_{n+1}, \mathbf{q}_{n+2}) = \mathscr{B}(\partial_t\mathbf{q}_n, \partial_t\mathbf{q}_{n+1}), \tag{7}$$

where and $\mathscr{A}$ and $\mathscr{B}$ are time-independent linear operators involving u-derivatives of $\delta\widetilde{\rho}_n$, whose expressions are given in Appendix A.

[1] The influence of $R > 1$ was discussed in the companion paper.

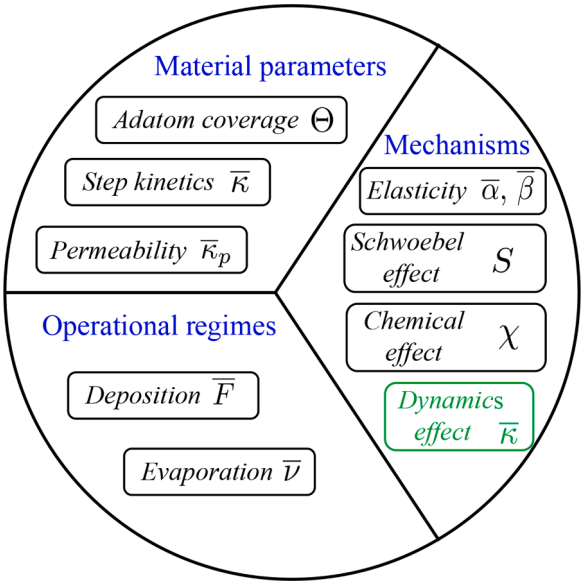

Fig. 1. Modification of the diagram on display in Fig. 4 of Part I, showing the complete set of factors governing the stability of step flow against bunching, including the dynamics effect as a stabilizing/destabilizing mechanism for different regimes, as measured by the step kinetics parameter $\overline{\kappa}$.

Floquet-wave analysis

The linear differential equations in (7) involve the spatial variable $\nu = u + n \in \mathbb{R}$, where $u \in (0,1)$ is the local variable and $n \in \mathbb{Z}$. They are translationally invariant, since the linear operators $\mathscr{A}$ and $\mathscr{B}$ are independent of n, i.e., they are invariant under m-terrace translations for all $m \in \mathbb{Z}$. This space periodicity of the differential operators allows us, according to the *Floquet-wave theory*, to write the solutions of (7) as $\delta\widetilde{\rho}_n(u,t) = \delta\widetilde{\rho}(u,t)\exp(ikn)$ and $\delta x_n(t) = \delta\widetilde{x}(t)\exp(ikn)$, with $k \in [-\pi,\pi]$ the wavenumber. Moreover, the system is autonomous, i.e., the linear operators $\mathscr{A}$ and $\mathscr{B}$ in (7) are time-independent, which leads to solutions of the form $\delta\widetilde{\rho}(u,t) = \delta\widehat{\rho}(u)\exp(\lambda t)$ and $\delta\widetilde{x}(t) = \delta\widehat{x}\exp(\lambda t)$, where λ is the growth rate of the perturbation whose wavenumber is k. Combining these results, the solutions of (7) can be written as

$$\delta x_n(t) = \delta\widehat{x}\exp(ikn+\lambda t), \quad \delta\widetilde{\rho}_n(u,t) = \delta\widehat{\rho}(u)\exp(ikn+\lambda t). \tag{8}$$

Inserting (8) in (7) yields a generalized eigenvalue problem associated with each wavenumber k,

$$\widehat{\mathscr{A}}_k\widehat{\mathbf{q}} = \lambda\widehat{\mathscr{B}}_k\widehat{\mathbf{q}}, \tag{9}$$

where $\widehat{\mathbf{q}}(u) := (\delta\widehat{x},\delta\widehat{\rho}(u))$, and $\widehat{\mathscr{A}}_k$ and $\widehat{\mathscr{B}}_k$ are linear operators derived from $\mathscr{A}$ and $\mathscr{B}$, whose corresponding expressions are furnished in Appendix A.

As detailed in Appendix B, the numerical resolution of (9) for a given k furnishes a set of complex eigenvalues $\mathscr{E}(k)$, from which we obtain the critical growth rate $\mathrm{Re}(\lambda(k))$ where $\lambda(k)$ is the eingenvalue in $\mathscr{E}(k)$ with maximum real part. The train of equidistant steps is linearly stable with respect to bunching when $\mathrm{Re}(\lambda(k)) < 0$ for all $k \in [-\pi,\pi]$ and unstable otherwise. Since $\lambda(-k) = \overline{\lambda(k)}$, $\mathrm{Re}(\lambda(k))$ needs only to be studied on $[0,\pi]$, which provides the dispersion relation of the problem at hand.

3. Results

In a departure from its quasistatic counterpart of Part I, the stability analysis presented in Section 2 captures the effect of dynamics on step bunching. Specifically, the inclusion of the dynamical terms in the stability analysis reveals a new stabilizing/destabilizing mechanism, which we refer to as *the dynamics effect*.

We first characterize, in Section 3.1, the specific effect of dynamics on stability by isolating it from the other mechanisms, which were investigated in Part I. In Section 3.2, we find how the dynamics effect scales with the material and operational parameters Θ, $\overline{F}$, and $\overline{\nu}$, which allows us to discuss its importance relative to the other mechanisms. Finally, in Section 3.3, we show how accounting for dynamics modifies the stability predictions associated with the classical mechanisms.

To highlight the changes brought by the general theory, the complete set of factors that govern the stability against bunching, including the dynamics effect is displayed in Fig. 1. In this section, we do not yet consider any particular material; instead, we select generic values or ranges for the material and operational parameters. These values are in line with the estimations for materials like Si and GaAs, as detailed in Appendix C.

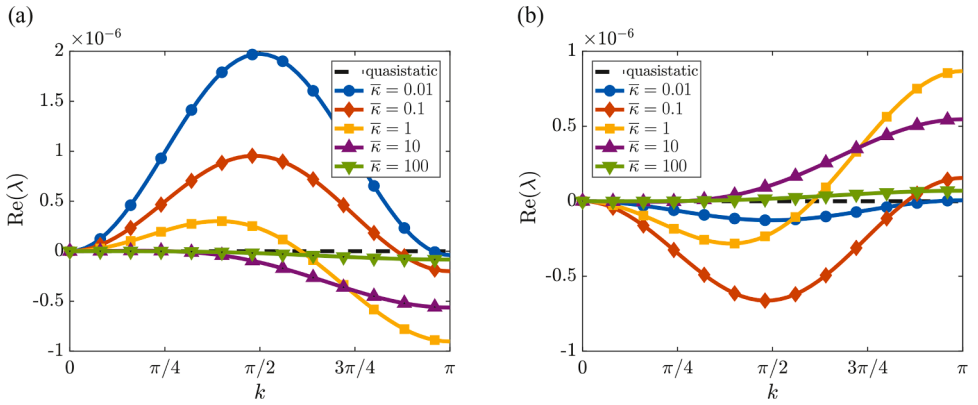

Fig. 2. Dispersion curves: $\mathrm{Re}(\lambda)$ vs. wavenumber k, showing the influence of the dynamics effect on stability in the absence of elastic step interactions ($\overline{\alpha} = \overline{\beta} = 0$), chemical effect ($\chi = 0$), step permeability ($\overline{\kappa}_p = 0$), and attachment/detachment bias ($S = 1$), under: (a) deposition ($\overline{F} = 0.01, \overline{\nu} = 0$) and (b) evaporation ($\overline{\nu} = 0.01, \overline{F} = 0$). Results are plotted for five different values of step kinetics $\overline{\kappa}$ and compared with the quasistatic case, where $\mathrm{Re}(\lambda(k)) = 0, \ \forall k \in [0, \pi]$.

Table 1
Effects of each of the basic mechanisms, including dynamics, on the onset of the bunching instability. ES refers to the Ehrlich–Schwoebel effect, iES to its inverse, CE to the chemical effect, DDE to dipole-dipole elastic interactions, MME to their monopole-monopole counterparts and DYN to the dynamics effect. $\mathscr{S}$ stands for stabilizing and $\mathscr{D}$ for destabilizing.

	ES $S > 1$	iES $S < 1$	CE χ	DDE $\overline{\alpha}$	MME $\overline{\beta}$	DYN $\overline{\kappa} \ll 1$	DYN $\overline{\kappa} \gg 1$
Deposition	$\mathscr{S}$	$\mathscr{D}$	$\mathscr{D}$	$\mathscr{S}$	$\mathscr{D}$	$\mathscr{D}$	$\mathscr{S}$
Evaporation	$\mathscr{D}$	$\mathscr{S}$	$\mathscr{S}$	$\mathscr{S}$	$\mathscr{D}$	$\mathscr{S}$	$\mathscr{D}$

3.1. Effect of dynamics in the deposition and evaporation regimes

To analyze the effect of dynamics on stability, we formally "disable" the other stabilizing/destabilizing mechanisms. Specifically, we "turn off" elastic step-step interactions by setting $\overline{\alpha} = \overline{\beta} = 0$, the chemical effect by taking $\chi = 0$, and the Ehrlich–Schwoebel effect by choosing $S = 1$. Furthermore, steps are assumed impermeable ($\overline{\kappa}_p = 0$). The effect of dynamics on the different modes of bunching is given by the dispersion curves: $\mathrm{Re}(\lambda(k))$ as a function of the wavenumber k. As can be seen in Fig. 2,

the step kinetics $\overline{\kappa}$ plays a crucial role in the stabilizing/destabilizing influence of dynamics.

Under deposition (Fig. 2(a)), dynamics has a stabilizing effect for high values of $\overline{\kappa}$ (with $\overline{\kappa} \gg 1$ corresponding to the diffusion-limited regime) and a destabilizing effect for low values of $\overline{\kappa}$ (with $\overline{\kappa} \ll 1$ associated with the kinetic-limited regime).[2] Interestingly, in the latter case the most unstable modes are those with intermediate wavelength ($k \sim \pi/2$). This feature of the destabilizing effect of dynamics is in stark contrast with the fact that the other destabilizing mechanisms predominantly affect step-pairing (cf. the discussion in Section 4 of Part I), and this is the reason for the special behavior in the maturing phase of the bunches when these are triggered by the dynamics effect [2]. Note that the effect of step kinetics is reversed during evaporation (Fig. 2(b)), where low values of $\overline{\kappa}$ (i.e., $\overline{\kappa} \ll 1$) correspond to a stabilizing effect while intermediate and high values of $\overline{\kappa}$ (i.e., $\overline{\kappa} \gtrapprox 1$) are destabilizing. These results are summarized in Table 1, which completes Table 1 of the companion paper.

3.2. Scalings related to dynamics

In the presence of the dynamics effect and in the absence of all the other stabilizing/destabilizing mechanisms, a parametric study reveals that varying $\overline{F}$, $\overline{\nu}$, and Θ does not alter the shape of the dispersion curve. Instead, these parameters act as scaling factors for $\mathrm{Re}(\lambda)$. As can be seen in Fig. 3, which exhibits the dispersion curves for different values of $\overline{F}$ and Θ under deposition, and of $\overline{\nu}$ and Θ under evaporation, the growth rate scales linearly with the deposition/evaporation rates ($\mathrm{Re}(\lambda) \propto \overline{F}$ and $\mathrm{Re}(\lambda) \propto \nu$) and quadratically with the adatom coverage ($\mathrm{Re}(\lambda) \propto \Theta^2$). The scalings of the dynamics contribution to stability with $\overline{F}$, $\overline{\nu}$ and Θ are summarized in Table 2, thus

[2] Recall from Part I that the notions of kinetic-limited and diffusion-limited regimes refer to the two kinetic processes at play during growth/evaporation by step flow: adatom attachment/detachment (a/d) at steps and their diffusion on terraces. $\overline{\kappa} := \kappa_- L_0/D$ can be seen as the ratio of a characteristic step kinetic velocity κ_- to a characteristic diffusion velocity D/L_0. Thus, $\overline{\kappa} \ll 1$ corresponds to situations where a/d is the limiting kinetic process and $\overline{\kappa} \gg 1$ to cases where terrace diffusion is limiting.

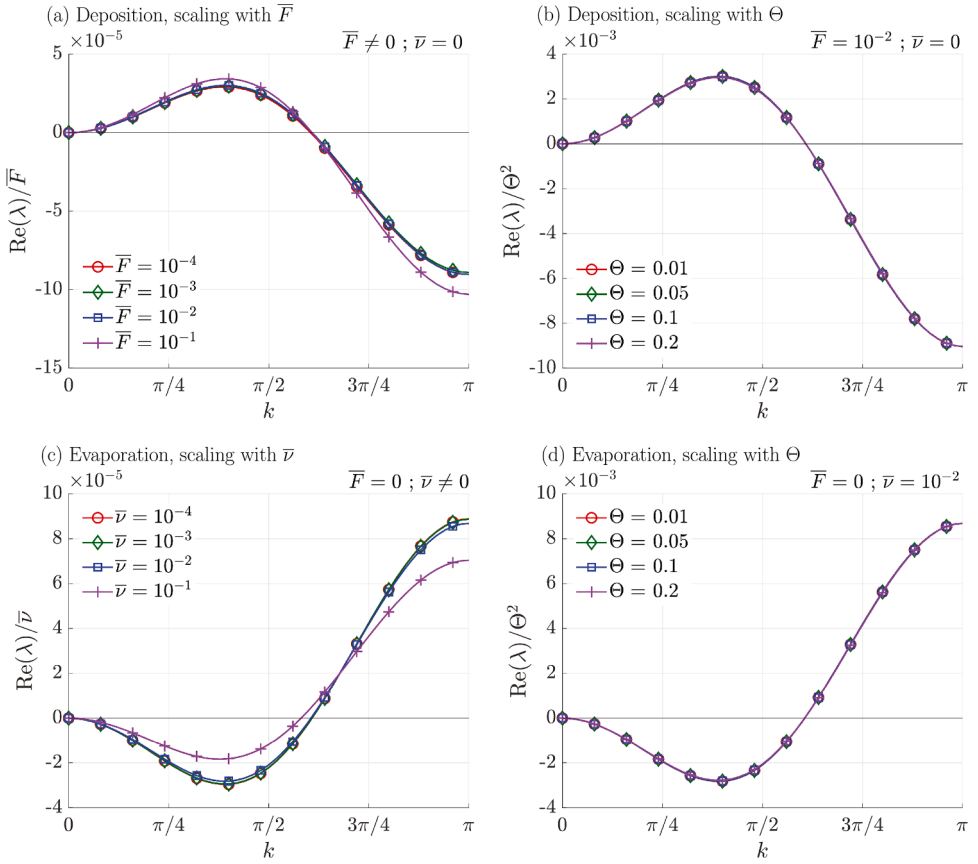

Fig. 3. Scaling of the dispersion curves $\mathrm{Re}(\lambda(k))$ with: (a) the deposition flux $\overline{F}$, (b,d) the adatom coverage Θ, and (c) the evaporation rate $\overline{\nu}$. The results, calculated for $\overline{\kappa} = 1$, show the influence of the dynamics on stability in the absence of elastic step-step interactions ($\overline{\alpha} = \overline{\beta} = 0$), chemical effect ($\chi = 0$), step permeability ($\overline{\kappa}_p = 0$), and attachment/detachment asymmetry ($S = 1$). In (a) and (c), $\Theta = 0.01$.

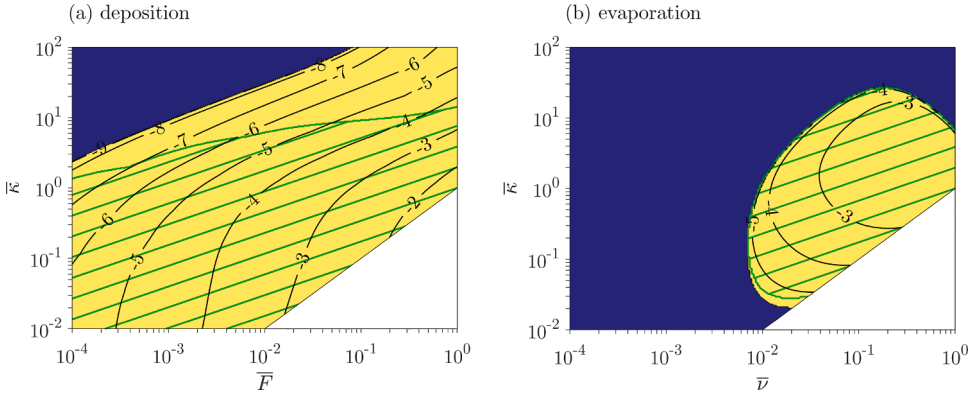

Fig. 4. Stability diagrams with respect to step bunching in the presence of the dynamics effect and dipole-dipole elastic interactions under (a) deposition ($\overline{\nu} = 0$) and (b) evaporation ($\overline{F} = 0$). In both cases, $\Theta = 0.2$, $\overline{\alpha} = 10^{-4}$, and $\overline{\beta} = 0$, while step permeability, the Ehrlich–Schwoebel barrier, and the chemical effect are ignored ($\overline{\kappa}_p = 0$, $S = 1$, and $\chi = 0$). Blue, yellow, and green hatched domains correspond to the *stable, unstable*, and *significantly unstable* regions, respectively. Recall, for comparison, that in the quasistatic regime step flow is stable (blue domain) everywhere. The white areas correspond to regions where the step-flow regime breaks down. (For interpretation of the references to colour in this figure legend, the reader is referred to the web version of this article.)

Table 2
The scalings of the contributions of the different mechanisms to the perturbation growth rate with the operating parameters $\overline{F}$ and $\overline{\nu}$ and the adatom coverage Θ. ES/iES refers to the Ehrlich–Schwoebel barrier or its inverse, CE to the chemical effect, E to the elastic step-step interactions, and DYN to the dynamics effect. The contribution of each mechanism scales as $\mathrm{Re}(\lambda)\propto\overline{F}^{a}\Theta^{b}$ under deposition and $\mathrm{Re}(\lambda)\propto\overline{\nu}^{a}\Theta^{b}$ under sublimation, with the exponents a and b given in the table.

	ES/iES	CE	E	DYN
	S	χ	$\overline{\alpha},\overline{\beta}$	$\overline{\kappa}$
a (for $\overline{F},\overline{\nu}$)	1	1	0	1
b (for Θ)	1	2	1	2

completing Table 2 of the companion paper.

3.3. Modification of the quasistatic approximation stability results

In this section, we examine successively the modifications caused by the dynamics effect on the stability results when: (i) elasticity is included in the form of dipole-dipole interactions (i.e., for homoepitaxy), (ii) the Ehrlich–Schwoebel barrier is accounted for, and (iii) the thermodynamically necessary chemical effect is incorporated. To this end, we compare the stability diagrams showing the domain of stable step propagation vs. that of step bunching as a function of the material and operational parameters.

To be more accurate in the predictions of bunching, we introduce the concept of *significant instability* corresponding to the regions where the growth rate $\lambda_{\max} := \max_{k\in[0,\pi]}\mathrm{Re}(\lambda(k))$ is sufficiently large for the bunching instability to develop during the deposition/evaporation of a thousand monolayers (i.e., a few hundred nanometers). Indeed, there are cases where $\lambda_{\max}$ is positive (indicating unstable step propagation) but with values so small that the step bunches develop only after deposition/evaporation of a number of monolayers beyond what is typically observed in experiments. We define the regime of *significant instability* via the condition $\lambda_{\max}\tau \geq 1$, where τ is the dimensionless time associated with the deposition (evaporation) of a thousand monolayers, i.e., $\tau_{dep} = 1000\ /\overline{F}\Theta$ ($\tau_{eva} = 1000/\overline{\nu}\Theta$).[3]

We conclude this section with a discussion of the validity of the quasistatic approximation in the regimes of slow deposition ($\overline{F}\Theta \ll 1$) and evaporation ($\overline{\nu}\Theta \ll 1$), where this approximation is classically and, as we will see, unduly invoked in the literature [e.g., 21,24].

Elasticity (dipole-dipole interactions)

We first consider, in Fig. 4, the influence of the dynamical terms on the stability of steps interacting through dipole-dipole elastic interactions (as happens during homoepitaxy, with $\overline{\alpha} = 10^{-4}$ and $\overline{\beta} = 0$), while step permeability, the Ehrlich–Schwoebel barrier, and chemical effects are all ignored ($\overline{\kappa}_p = 0$, $S = 1$, and $\chi = 0$). Blue and yellow domains correspond to the stable ($\lambda_{\max} < 0$) and unstable ($\lambda_{\max} > 0$) regions. In the unstable domain, isolines display $\log_{10}(\lambda_{\max})$, indicating the magnitude of the most critical growth rate, and the hatched green region corresponds to the domain of significant instability, as defined earlier. The white area corresponds to combinations $(\overline{\kappa},\overline{F})$ and $(\overline{\kappa},\overline{\nu})$ that are not within the hypothesis of validity of (1), as they lead to terrace adatom densities that significantly depart from their equilibrium values (see Section 2.1 of Part I). In practice, we expect a breakdown of the step-flow regime in this region, which renders the question of stability irrelevant. For comparison of these stability diagrams with the quasistatic case, recall that in the latter, because of the stabilizing effect of elasticity, step propagation is stable under both deposition and evaporation for all parameter values.

In Fig. 4(a), the stability diagram under deposition in the $(\overline{F},\overline{\kappa})$ parameter space is shown, when the dynamical terms are accounted for. With $\overline{\alpha} = 10^{-4}$ (which is the order of magnitude of the strength of elastic interactions for a terrace width of 20 nm, see Appendix C), we can see a region of instability, which is a manifestation of the breakdown of the quasistatic approximation. Indeed, although we are in the regime $\overline{F}\Theta \ll 1$, the dynamic terms have a significant effect on stability.

Finally, Fig. 4(b) displays the stability diagram under evaporation in the $(\overline{\nu},\overline{\kappa})$ space, when dynamic terms are included, calculated for the same parameters as Fig. 4(a) ($\overline{\alpha} = 10^{-4}, \overline{\beta} = 0, S = 1$, $\overline{\kappa}_p = 0$, $\chi = 0$, and $\Theta = 0.2$). Again, as a result of the presence of the dynamical terms, an unstable region appears for $\overline{\nu} > 10^{-2}$ and $\overline{\kappa}$ in the intermediate range between 0.1 and 10, corresponding to the values of $\overline{\kappa}$ for which the destabilizing effect of dynamics is the most important under evaporation, cf. Fig. 2(b).

Schwoebel effect

Next, we consider the interplay of the dynamical effect with the Ehrlich–Schwoebel barrier, while all the remaining mechanisms are disabled: $\overline{\alpha} = 0$, $\overline{\beta} = 0$, $\chi = 0$, $\overline{\kappa}_p = 0$.

[3] Indeed, under deposition ($\overline{\nu} = 0$), the deposition time T_d for one monolayer is given by the equality, for an arbitrary surface area A, between that surface area and the one covered by the flux F of adatoms during the time T_d, i.e., $A = Fa^2T_dA$. This furnishes $T_d = 1/Fa^2$, and the dimensionless deposition time for one monolayer is $1/\overline{F}\Theta$. Similarly, under evaporation ($\overline{F} = 0$), one can easily show that the dimensionless time associated with the evaporation of one monolayer is $1/\overline{\nu}\Theta$.

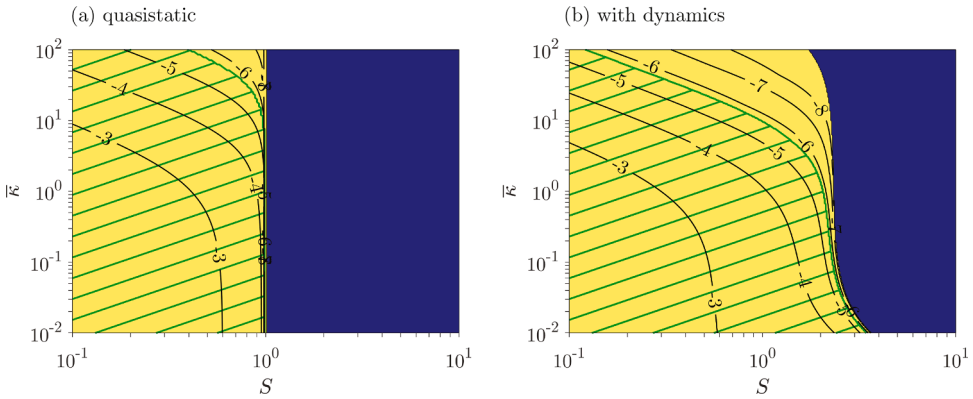

Fig. 5. Influence of dynamics on the stability diagram of the Schwoebel effect under deposition: (a) Schwoebel effect in the quasistatic regime, (b) Schwoebel effect with dynamics. In both cases $\overline{F} = 10^{-2}$ and $\Theta = 0.2$, while all other mechanisms are disabled ($\overline{\alpha} = 0, \overline{\beta} = 0, \overline{\kappa}_p = 0, \chi = 0$). Colors and isolines have the same meaning as in Fig. 4.

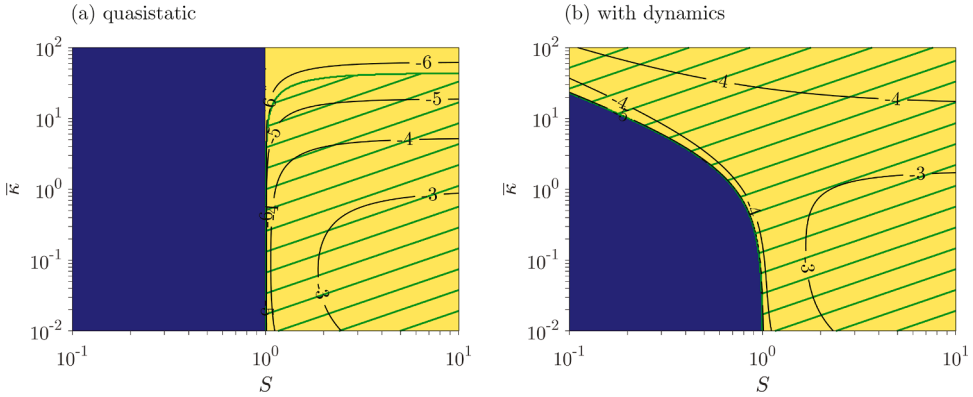

Fig. 6. Influence of dynamics on the stability diagram of the Schwoebel effect under evaporation. (a) Schwoebel effect in the quasistatic regime, (b) Schwoebel effect accounting for dynamics. In both cases $\overline{\nu} = 10^{-2}$ and $\Theta = 0.2$, while all other mechanisms are disabled: $\overline{\alpha} = 0, \overline{\beta} = 0, \overline{\kappa}_p = 0, \chi = 0$. See Fig. 4 for the legends of colors and isolines.

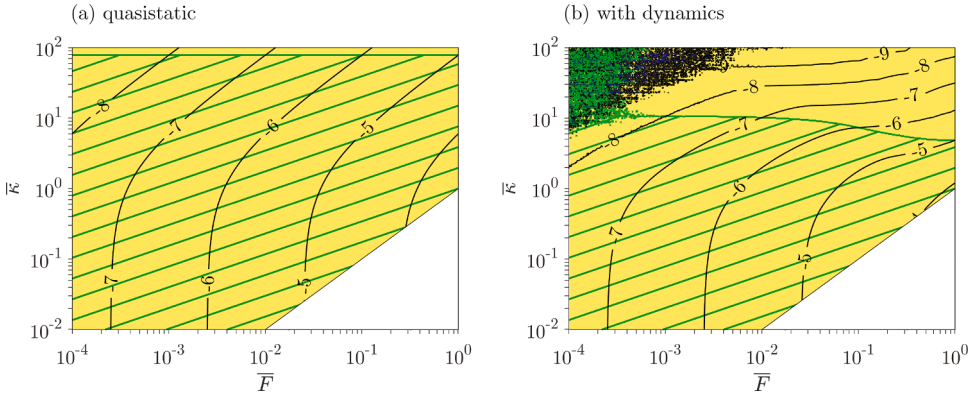

Fig. 7. Influence of dynamics on the stability diagram of the chemical effect under deposition. (a) chemical effect in the quasistatic regime, (b) chemical effect in the presence of dynamical terms. In both cases $\Theta = 0.01$, with the remaining mechanisms disabled: $S = 1, \overline{\alpha} = 0, \overline{\beta} = 0$, and $\overline{\kappa}_p = 0$. See Fig. 4 for the legends of colors and isolines.

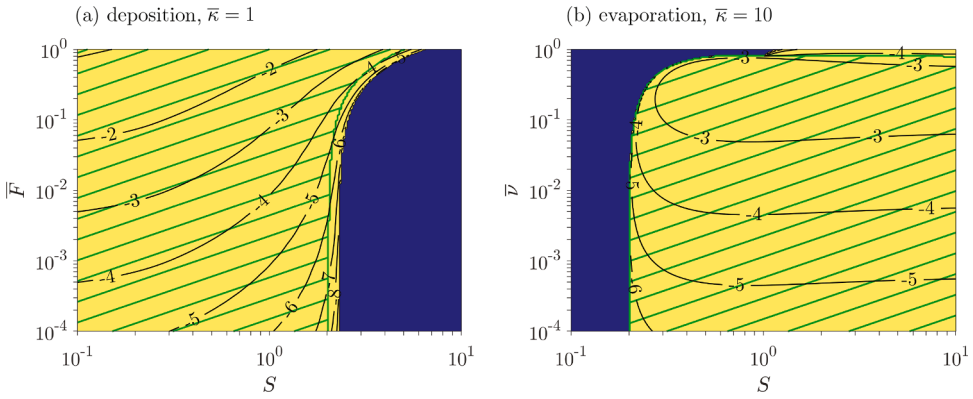

Fig. 8. Influence of the depositon and evaporation rates on the stability diagram combining Schwoebel and dynamics effects. (a) under deposition with $\overline{\kappa} = 1$, and (b) under evaporation with $\overline{\kappa} = 10$. In both cases $\Theta = 0.01$ while the other mechanisms are disabled: $\overline{\alpha} = 0$, $\overline{\beta} = 0$, $\chi = 0$ and $\overline{\kappa}_p = 0$. See Fig. 4 for the legends of colors and isolines.

In Fig. 5(a), we show the stability diagram associated with the Schwoebel effect under the quasistatic approximation for the deposition case, with stable growth for $S > 1$ and unstable growth for $S < 1$. As can be seen on Fig. 5(b), the effect of dynamics is to extend the significantly unstable region beyond $S = 1$ for slow step kinetics ($\overline{\kappa} < 1$) and reduce it below $S = 1$ for fast step kinetics ($\overline{\kappa} > 10$), a change that ensues from the stabilizing and destabilizing effects of dynamics shown on Fig. 2(a). In addition, note that the influence on stability of the Schwoebel effect is substantially modified by dynamics in the very regime of small deposition rate (here $\overline{F}\Theta = 2 \times 10^{-3} \ll 1$).

Similarly, under evaporation (Fig. 6), dynamics modifies the stability diagram of the Schwoebel effect with an extension of the unstable region in the domain $S < 1$ in the regime of fast step kinetics ($\overline{\kappa} > 1$).

Chemical effect

The chemical effect, which couples the diffusion fields on all terraces, yields, in the quasistatic regime, an unstable step flow under deposition and a stable one under evaporation (cf. Table 1 and Section 4.2 of the companion paper). Fig. 7 shows that under deposition, dynamics reduces the domain of significant instability where $\overline{\kappa} \gg 1$, which is consistent with its stabilizing effect in this regime (see Fig. 2(a)). Nonetheless, no stable domain (in the sense of $\lambda_{\max} < 0$) appears because of the marginal instability of dynamics for long wavelength modes $k \to 0$ when $\overline{\kappa} \gg 1$.

Under evaporation, dynamics has a destabilizing effect for $\overline{\kappa} \gg 1$, which, however, is not strong enough to reverse the stability of the chemical effect. As a result, both under the quasistatic approximation and in the presence of the dynamical effect, the stability diagram associated with the chemical effect under evaporation shows stable step flow for all parameter values.

Relative importance of dynamics for different values of $\overline{F}$ and Θ

The above discussion of the interplay between the dynamics effect and the three fundamental mechanisms of step-flow growth (Fig. 1) shows that even in the regimes of slow deposition and slow evaporation (defined by $\overline{F}\Theta \ll 1$ and $\overline{\nu}\Theta \ll 1$, respectively), where the quasistatic approximation is invoked in the literature, the effect of dynamics is far from negligible. While this already points to the failure of the quasistatic approximation, we can still wonder whether the effect of dynamics becomes negligible as $\overline{F} \to 0$ or $\overline{\nu} \to 0$. As we show below, it is not so in general, which confirms that the postulate according to which the quasistatic approximation is valid for slow deposition/evaporation is fundamentally erroneous. To discuss the relative importance of dynamics for vanishingly small deposition/evaporation rates, we go back to the scaling of the different mechanisms with $\overline{F}$, $\overline{\nu}$, and Θ, given in Table 2.

Considering first elasticity versus dynamics, we note that the effect of elasticity is independent of the deposition/evaporation rate while that of dynamics is linear in this rate. As a result, the latter becomes negligible compared to the former as $\overline{F}, \overline{\nu} \to 0$ (see Fig. 4). Note however that this is not specific to dynamics, as the same conclusion is drawn when comparing the Schwoebel or chemical effects with elasticity. This scaling difference is the basis for the distinction between *energetic mechanisms* (elasticity) and *kinetic mechanisms* (Schwoebel, chemical, and dynamics effects).

Since the three kinetic mechanisms have the same scaling with $\overline{F}$ and $\overline{\nu}$, their relative importance remains unchanged as $\overline{F}, \overline{\nu} \to 0$. A numerical confirmation is afforded by the observation that the stability diagrams of Figs. 5 and 6 remain unchanged for values of $\overline{F}$ and $\overline{\nu}$ across multiple decades below $\overline{F}, \overline{\nu} = 10^{-1}$. To illustrate this point, Fig. 8

shows how the critical Schwoebel barrier (i.e., the value of S at which stability is reversed) varies with $\overline{F}$ under deposition and with $\overline{\nu}$ under evaporation. That this critical barrier is independent of $\overline{F}$ and $\overline{\nu}$ when these are below 0.1 shows that the effect of dynamics (relative to Schwoebel) remains significant for $\overline{F}, \overline{\nu} \to 0$. The same conclusion can be drawn from Fig. 7 when comparing the relative importance of dynamics on the chemical effect. In view of the above, it is clear that the conditions $\overline{F}\Theta \ll 1$ and $\overline{\nu}\Theta \ll 1$ (or even the more restrictive ones $\overline{F}\Theta \to 0$ and $\overline{\nu}\Theta \to 0$) are not sufficient to neglect the effect of dynamics. Whether dynamics contributes

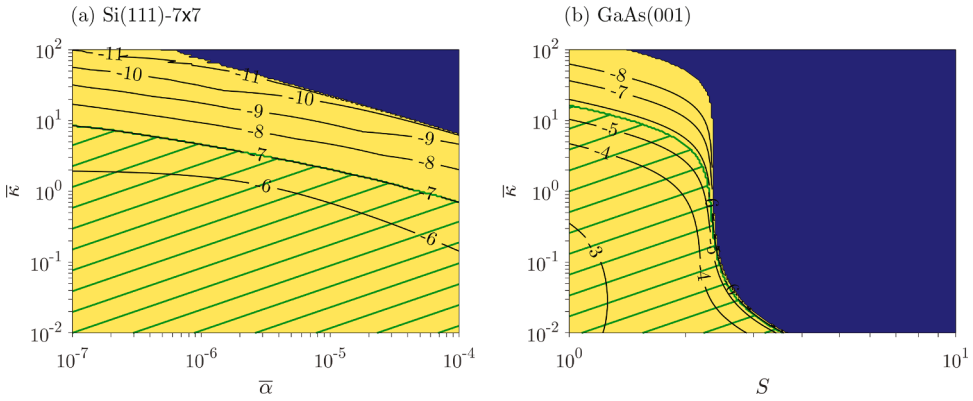

Fig. 9. (a) Stability diagrams for Si(111)-7 × 7 under deposition ($\overline{\nu} = 0$) combining elasticity, chemical and dynamics effects. The parameters are $\Theta = 0.01$, $\overline{F} = 10^{-2}$, $S = 1$, $\overline{\beta} = 0$, $\overline{\kappa}_p = 0$. (b) Stability diagrams for GaAs(001) under deposition ($\overline{\nu} = 0$) combining elasticity; Schwoebel, chemical, and dynamics effects. The parameters are $\Theta = 0.2$, $\overline{F} = 10^{-2}$, $\overline{\alpha} = 5 \times 10^{-6}$, $\overline{\beta} = 0$, $\overline{\kappa}_p = 0$. (see Fig. 4 for the legends of colors and isolines).

significantly or not to the (in)stability of the step flow for a particular experiment, depends, like for any other mechanism, on the whole set of material and operational parameters.

4. Reinterpreting some experiments

In this section, we consider two specific materials for which the bunching instability was observed under deposition and discuss how our thermodynamically consistent formulation of step flow, by accounting for the dynamics and chemical effects, may provide an alternative explanation of bunching to those proposed in the literature. To this end, we consider all the mechanisms together, whose strengths we estimate through an exhaustive survey of the existing experimental literature. (The reader is referred to Appendix C for the estimation of the various material parameters at play.)

The experiments we consider concern the epitaxial growth of GaAs(001) in the 600°C − 700°C range Hata et al., 1993; Ishizaki et al., 1994, 1996; Kasu and Fukui, 1992; Pond, 1994; Shinohara and Inoue, 1995 and Si(111)-7 × 7 around 700°C-780°C Omi et al., 2005, in which step bunching was observed under deposition. Recall that the stability analysis of the quasistatic BCF model, which precludes both dynamics and chemical effects, predicts that both the direct Ehrlich–Schwoebel effect ($S \geq 1$) and the elastic interactions between steps are stabilizing (see Section 4.2 of Part I, as well as Table 1). In this classical setting, observations of step bunching under deposition were first explained by invoking an inverse Schwoebel effect ($S < 1$) Ishizaki et al., 1996; Tejedor et al., 1998.

However, as acknowledged by several authors [28,38,43], an inverse ES barrier—which favors the attachment to a step of adatoms from its upper terrace—is difficult to justify both experimentally and theoretically. In particular, in GaAs(001) and Si(111)-7 × 7, the works that intended to measure the ES effect have concluded to the existence of a direct barrier ($S > 1$) in GaAs(001) and have lead to contradictory results for Si(111). Specifically, for GaAs(001) both atomistic simulations using empirical potentials Salmi et al., 1999 and experimental studies of island formation [20,39] have concluded to a direct ES barrier. On the other hand, for Si(111)-7 × 7, the observations of the denuded zones around steps Rogilo et al., 2013; Voigtlander et al., 1995, the measurements of the decay rates of island and holes under evaporation and deposition Ichimiya et al., 1996, and the measurements of the distributions over terraces of the nucleated islands under deposition Chung and Altman, 2002 have lead to contradictory conclusions, namely a direct ES barrier Ichimiya et al., 1996, an inverse ES effect Chung and Altman, 2002; Rogilo et al., 2013, and the absence of any asymmetry in the attachment of adatoms to steps [44].

This uncertainty has led theoreticians to consider new mechanisms to account for step bunching under deposition, such as the coupling between diffusing species (molecular precursors and adatoms) during the vapor phase epitaxy of GaAs(001) [28] and the fast diffusion of adatoms along steps of Si(111)-7 × 7 [29]. While these mechanisms are plausible, there is no clear evidence that they indeed cause the observed step bunching. In particular, step bunching on GaAs(001) is also observed in molecular beam epitaxy deposition experiments Pond, 1994, which do not involve precursors. Hence, the coupling with precursors cannot be invoked in relation to these experiments. In what follows, we show that the stability analysis of our step-flow model, which accounts for both chemical and dynamics effects, can explain the occurrence of step bunching under deposition.

4.1. Experiments on Ssi(111)-7 × 7

We start with a quick overview of the selection of material parameters for Si(111)-7 × 7 (further details are provided in Appendix C). First, the coefficient $\overline{\alpha}$ associated with elastic dipole-dipole interactions between steps can be estimated from the work of Stewart et al. [40]. It has a strong dependence on the terrace width: $\overline{\alpha} \propto L_0^{-3}$. In the experiments of Omi et al. Omi et al., 2005, L_0 typically varies between 10 nm and 60 nm, which corresponds to $\overline{\alpha}$ ranging from 2×10^{-7} and 4×10^{-4}. Next, as discussed above, the

very nature of the ES barrier in Si(111)-7 × 7 remains debated. We therefore assume symmetric attachment/detachment. Further, in the absence of precise information, we also consider a low value of adatom coverage, $\Theta = 0.01$, which is a conservative estimate insofar as it tends to minimize the influence of the chemical and dynamics effects. Moreover, the values of $\overline{F}$ and $\bar{\kappa}$ being either difficult to estimate or unknown, we take the intermediate value $\overline{F} = 10^{-2}$ (recall that changing $\overline{F}$ essentially changes the relative importance of elasticity, see Section 3.3) and allow values of $\bar{\kappa}$ that cover the different possible kinetic regimes (see Appendix C). Finally, in the absence of evidence that the steps of Si(111)-7 × 7 are permeable Chung and Altman, 2002, we take $\bar{\kappa}_p = 0$.

With the above estimated parameters, and in particular in the absence of an Ehrlich–Schwoebel barrier, the stability diagram of Fig. 9(a) shows that there exists a large green hatched zone of significant instability. While in this region, bunches develop within a thousand deposited monolayers, the more restrictive condition of one hundred monolayers for bunches to develop corresponds to the area below the "-6" isoline. In this region the speed of bunching is comparable to that observed in the experiments of Omi et al., 2005, in which bunches develop between 30 and 300 monolayers, thus indicating that the combined destabilizing chemical and dynamics effects are sufficiently strong to plausibly explain the instability in these experiments. In conclusion, a sufficient condition for the chemical and dynamics effects to induce an instability whose growth rate compares with that which is observed in the experiments of Omi et al. Omi et al., 2005 is that the step kinetics is slow ($\bar{\kappa} < 1$). Further experimental work directly assessing the step kinetics would help to identify the actual implication of the proposed mechanism.

4.2. Experiments on GgaAas(001)

We turn to the evaluation of the parameters for GaAs(001) at temperatures in the range 600°C − 700°C. Measurements and simulations of the Schwoebel barrier in GaAs(001) suggest a direct Schwoebel effect with estimates ranging from $S = 2$ to $S = 10$ at 600°C (see Appendix C). In addition, as detailed in Appendix C, the elastic interaction parameter is about $\bar{\alpha} = 5 \times 10^{-6}$ and the equilibrium adatom coverage is high, at around $\Theta = 0.2$. As discussed in Section 3.3, this implies that the chemical and dynamics effects are relatively influential. Finally, without any evidence for the existence of permeability in GaAs(001), we take $\bar{\kappa}_p = 0$.

With these parameters, the role played by elasticity is small and the stability diagram displayed in Fig. 9(b) results essentially from the combination of the Schwoebel, chemical, and dynamics effects. We can see that for $S > 2$ the Schwoebel effect prevails, which leads to stable step flow irrespective of the step kinetic regime. By contrast, when $S \leq 2$, significant step bunching is predicted for slow step kinetics ($\bar{\kappa} < 1$). Hence, the dynamics and chemical effects furnish a plausible explanation for the observed bunching on GaAs(001). Ultimately, the determining factor is the strength of the Schwoebel barrier, whose exact estimation is rendered difficult by the existence of different types of steps and of two simultaneously diffusing species, gallium and arsenic.

5. Discussion

Inadequacy of the quasistatic approximation

The comparison, *a posteriori*, of the stability results with and without dynamics (see Section 3.3) reveals the incorrectness of the hypothesis underlying the quasistatic approximation [as stated in, e.g., 21,24], according to which the dynamical terms are negligible in the slow deposition or evaporation regime, i.e., provided that $\overline{F}\Theta \ll 1$ or $\overline{\nu}\Theta \ll 1$.

Further, we can see from the stability problem itself that there is no *a priori* reason for neglecting the dynamics effect in the slow deposition and evaporation regimes. Indeed, determining the stability of the steady-state solution of (1) is tantamount to computing, for all wavelengths k, the eigenvalue of (9) with the largest real part. Yet, in the expressions given in Appendix A for the operators $\widehat{\mathscr{A}}_k$ and $\widehat{\mathscr{B}}_k$ that enter (9), we have highlighted in red the terms that derive from the dynamics effect in (1). Among these, we find in addition to terms proportional to $\overset{\circ}{V}$, which are of order $\overline{F}\Theta$ in the deposition regime and of order $\overline{\nu}\Theta$ under evaporation conditions, terms of order 0 in $\overline{F}\Theta$ or $\overline{\nu}\Theta$. Hence, even in the limit of vanishingly small deposition or evaporation rate, the generalized eigenvalue problem accounting for the dynamics effect differs from its counterpart in the quasistatic regime. This helps us understand why, as shown in Section 3.3, the stability results with and without dynamics differ significantly.

The different approaches to the effect of dynamics

In this paper, we have undertaken a thorough analysis of the effect of dynamics by investigating the stability of the complete step-flow problem (1). Our work follows previous studies that have accounted, at least partially, for dynamics by adopting different approaches. We now put these works in perspective, to highlight in particular the existence of two alternative methods to compute the stability of (1).

In Ranguelov and Stoyanov [32], the problem of step dynamics is tackled in the simplified framework of infinitely fast terrace diffusion ($D \to \infty$) and slow attachment/detachment kinetics (κ_- and κ_+ small but finite). In Ranguelov and Stoyanov [33], the same authors discuss the effect of dynamics on the problem of step bunching under electromigration. Finally, Ranguelov et al. [31] show experimental evidence that the dynamics effect may induce step bunching for sufficiently high deposition rates. The results presented in Fig. 4 are in qualitative agreement with those of Ranguelov and Stoyanov [32], where it should be noted that the limit case considered by these authors corresponds to $\bar{\kappa} \ll 1$. A detailed comparison of the stability predictions of our model when adatom electromigration is accounted for, with those of Ranguelov and Stoyanov [32] is presented elsewhere [1].

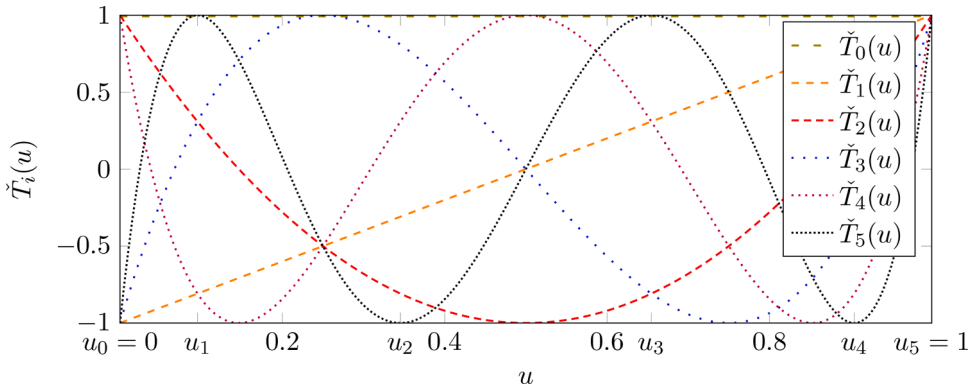

Fig. B.10. Representation of the first six Chebyshev polynomials $\check{T}_n$ along with the six Gauss-Lobatto points for $N = 5$.

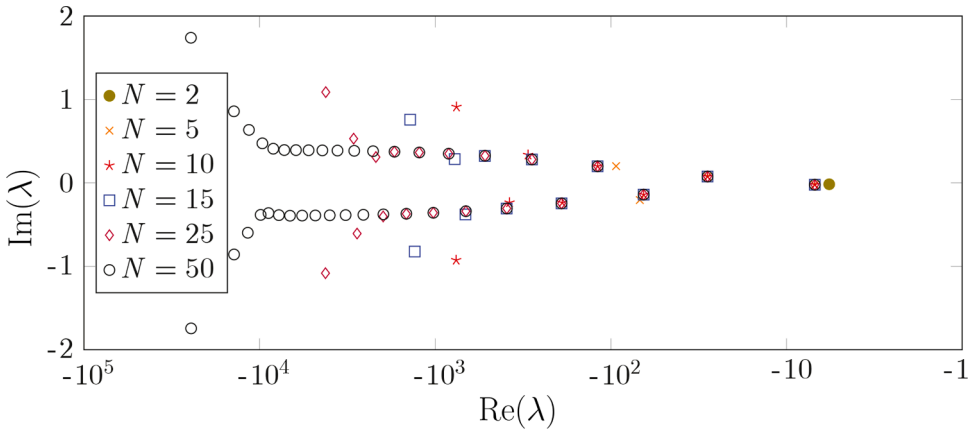

Fig. B.11. Evolution of the eigenvalue spectrum of (B.8) with the number N of discretization points for the set of parameters $\overline{F} = 10^{-2}$, $\overline{\nu} = 0$, $S = 1$, $\overline{\kappa} = 10$, $\overline{\kappa}_p = 0$, $\Theta = 0.01$, $\overline{\alpha} = 0$, $\overline{\beta} = 0$, and $k = \pi/2$. The logarithmic scale used on the abscissa is not wide enough to include the leading eigenvalue $-1.1271 \cdot 10^{-7} + 1.0000 \cdot 10^{-4} i$.

Other works [4,8,27] have considered the role of dynamics in free-boundary problems similar to (1). In Pierre-Louis [27] and Dufay et al. [4], in order to circumvent the mathematical difficulty that the transient term $\partial_t \rho_n$ in $(1)_1$ introduces in the stability analysis, the authors have solely accounted for the advective component of the transient term.[4] While this approach seems to yield the correct stability results for $\overline{F}, \overline{\nu} \to 0$, we have found several cases, still in the regime of slow deposition or evaporation, where the stability results derived from this simplified formulation differ significantly from the general ones. Indeed, in the absence of an asymptotic analysis showing that the transient terms can be neglected, our results advocate for keeping all the dynamical terms, without resorting to unjustified simplifications.

A treatment of the effect of dynamics on the step stability problem, including the transient term in $(1)_1$, is developed in Ghez et al. [6], 7] and Keller et al. [19]. In these works, the authors write the perturbation equations on the domain of the steady-state solution and correct the inadequacy of the domain of definition through Taylor expansions of the boundary conditions about the steady-state positions of the steps. Using the terminology in place in stability problems involving fluid-structure interactions—where the same issue of both function and domain perturbation arises—their approach is referred to as the *transpiration method*, by contrast with ours, which makes use of the *arbitrary Lagrangian-Eulerian formulation* [see e.g., 5]. However, in the formulation by Ghez et al. [6], 7], Keller et al. [19], the dynamics terms are missing from the boundary conditions $(1)_{2,3}$. These terms were only included in the step-flow problem in later works [see, e.g., [4,27,32]].

[4] Specifically, the term $\partial_t \rho_n$ can be decomposed into a convective component and a transient one by introducing the change of variable $\widetilde{x} := x - (n + \overset{\circ}{V} t)$. Letting $\widetilde{\rho}_n(\widetilde{x}, t) := \rho_n(\widetilde{x} + n + \overset{\circ}{V} t, t)$, the time derivative of ρ_n is rewritten as $\partial_t \rho_n = \partial_t \widetilde{\rho}_n - \overset{\circ}{V} \partial_x \widetilde{\rho}_n$. In Pierre-Louis [27] and Dufay et al. [4], only the advective term $-\overset{\circ}{V} \partial_x \widetilde{\rho}_n$ is accounted for, while the time derivative $\partial_t \widetilde{\rho}_n$ is neglected in $(1)_1$. Similarly, in the boundary conditions $(1)_{2,3}$ at the steps, the terms $-\rho_n^- \dot{x}_{n+1}$ and $\rho_n^+ \dot{x}_n$ are replaced by $-\rho_n^- \overset{\circ}{V}$ and $\rho_n^+ \overset{\circ}{V}$, thus neglecting the perturbations in the step positions about the principal velocity $\overset{\circ}{V}$.

More recently, making use again of the transpiration method, Gillet [8] addressed the stability of steps, with proper account for all the dynamical terms. However, the resulting effect of dynamics on stability is not discussed in this work, as Gillet [8] simply notes that the dynamics effect may destabilize the steps under deposition. By contrast, in Section 3, we furnish a complete characterization of the effect of dynamics and of its importance relative to the other stabilizing/destabilizing mechanisms. In particular, we point out there the fundamental role of $\bar{\kappa}$ for understanding the effect of dynamics on stability.

To conclude this discussion, we mention the work of Sekerka [36], which is concerned by the stability of a planar solidification front. Although this problem is different from ours, it shares similarities in the formalism, being also a Stefan-like problem. In this work, the author addressed the influence of the equivalent to our "dynamics effect" on the stability. However, as in the work of Ghez et al. [6] on the step-flow problem, the terms related to the advective current are missing from the boundary conditions. This omission opens the road for revisiting the effect of dynamics on stability in other problems of a similar nature.

6. Summary and concluding remarks

In this paper, we have investigated the onset of the bunching instability on vicinal surfaces without recourse to the quasistatic approximation, thereby unraveling the effect of dynamics. We find that both under deposition and evaporation, dynamics can be stabilizing or destabilizing depending on the value of $\bar{\kappa}$ (which expresses the ratio of step attachment/detachment kinetics to terrace diffusion kinetics). In examining how the strength of the dynamics effect varies with the material and operational parameters, we show that the effect of dynamics on stability scales linearly with the deposition/evaporation rate (as do the Schwoebel and chemical effects) and quadratically with the adatom coverage (as does the chemical effect).

When combined with the other stabilizing/destabilizing mechanisms, we find that dynamics significantly modifies the stability diagrams and that its influence does not necessarily decrease for small deposition/evaporation rates. From a theoretical perspective, this shows the inadequacy of the quasistatic approximation as usually invoked in the literature. From the experimental viewpoint, it calls for reinterpreting the cause of step bunching observed in some experiments.

In relation to this last point, we have surveyed several experimental works to estimate the physical parameters that enter the thermodynamically consistent formulation of the step-flow problem and have found that dynamics provides a plausible explanation for some cases of step bunching observed in GaAs(001) and Si(111)-7 $\times$ 7. This explanation provides an alternative to the additional physical mechanisms invoked in the literature to account for step bunching. To determine with certainty the mechanisms that are actually involved in particular occurrences of bunching, one needs to consider the long-term evolution of the bunches. Such an analysis was sketched in Guin et al. [9] and fully developed in Benoit-Maréchal et al. [2].

Declaration of Competing Interests

The authors declare that they have no known competing financial interests or personal relationships that could have appeared to influence the work reported in this paper.

CRediT authorship contribution statement

L. Guin: Formal analysis, Investigation, Methodology, Software, Writing – original draft, Writing – review & editing, Funding acquisition. **M.E. Jabbour:** Conceptualization, Methodology, Supervision, Writing – original draft, Writing – review & editing, Funding acquisition. **L. Shaabani-Ardali:** Methodology, Software, Writing – original draft. **N. Triantafyllidis:** Conceptualization, Methodology, Supervision, Writing – review & editing.

Declaration of Competing Interest

The authors declare no conflict of interest.

Acknowledgment

This work is supported by the "IDI 2015" project funded by the IDEX Paris-Saclay under grant ANR-11-IDEX-0003-02. The authors thank L. Benoit-Maréchal for fruitful discussions.

Appendix A. Expressions of the linear stability operators

Expressions of the operators $\mathscr{A}$ and $\mathscr{B}$

The linear operator $\mathscr{A}$ introduced in (7) is defined by

$$\mathscr{A}\begin{pmatrix}\\ \mathbf{q}_{n-1},\mathbf{q}_n,\mathbf{q}_{n+1},\mathbf{q}_{n+2}\\ \\ \end{pmatrix} = \begin{pmatrix} A_1^1(u)\,(\delta x_n-\delta x_{n+1}) \\ A_2^1\,\delta x_n + A_2^{1'}\,\delta x_{n+1} + A_2^{1''}\,\delta x_{n+2} \\ A_3^1\,\delta x_{n-1} + A_3^{1'}\,\delta x_n + A_3^{1''}\,\delta x_{n+1} \\ A_4^1\,(\delta x_{n-1}-2\delta x_n+\delta x_{n+1}) \end{pmatrix} + \begin{pmatrix} A_1^2\,\delta\widetilde{\rho}_n(u,t) \\ A_2^2\,\delta\widetilde{\rho}_{n+1}^{+} + A_2^{2'}\,\delta\widetilde{\rho}_n^{-} \\ A_3^2\,\delta\widetilde{\rho}_n^{+} + A_3^{2'}\,\delta\widetilde{\rho}_{n-1}^{-} \\ A_4^2\,\delta\widetilde{\rho}_n^{+} + A_4^{2'}\,\delta\widetilde{\rho}_{n-1}^{-} \end{pmatrix} + \begin{pmatrix} \overset{\circ}{V}\partial_u\delta\widetilde{\rho}_n(u,t) \\ \left(\partial_u\delta\widetilde{\rho}_n\right)^{-} \\ -\left(\partial_u\delta\widetilde{\rho}_n\right)^{+} \\ 0 \end{pmatrix} + \begin{pmatrix} \partial_{uu}\delta\widetilde{\rho}_n(u,t) \\ 0 \\ 0 \\ 0 \end{pmatrix}, \tag{A.1}$$

where

$$\begin{cases} A_1^1(u) = & 2\nu\overset{\circ}{\widetilde{\rho}}(u) - 2F - \overset{\circ}{V}\overset{\circ}{\widetilde{\rho}}(u), \\ A_2^1 = & \overline{\kappa}\left(1+3\overline{\alpha}-\overline{\beta}\right) + \left(\overline{\kappa}_p+\overline{\kappa}\chi\Theta\right)\overset{\circ}{\widetilde{\rho}}(0) - \left(\overline{\kappa}(1+\chi\Theta)+\overline{\kappa}_p+\overset{\circ}{V}\right)\overset{\circ}{\rho}(1), \\ A_2^{1'} = & -\overline{\kappa}\left(1+6\overline{\alpha}-2\overline{\beta}\right) - \left(\overline{\kappa}_p+\overline{\kappa}\chi\Theta\right)\overset{\circ}{\widetilde{\rho}}(0) + \left(\overline{\kappa}(1+\chi\Theta)+\overline{\kappa}_p+\overset{\circ}{V}\right)\overset{\circ}{\rho}(1), \\ A_2^{1''} = & \overline{\kappa}\left(3\overline{\alpha}-\overline{\beta}\right), \quad A_3^1 = \overline{\kappa}S\left(3\overline{\alpha}-\overline{\beta}\right), \\ A_3^{1'} = & \overline{\kappa}S\left(1-6\overline{\alpha}+2\overline{\beta}\right) + \left(\overline{\kappa}_p-\overline{\kappa}S\chi\Theta\right)\overset{\circ}{\widetilde{\rho}}(1) + \left(\overline{\kappa}S+(\chi\Theta-1)-\overline{\kappa}_p+\overset{\circ}{V}\right)\overset{\circ}{\rho}(0), \\ A_3^{1''} = & -\overline{\kappa}S\left(1-3\overline{\alpha}+\overline{\beta}\right) - \left(\overline{\kappa}_p-\overline{\kappa}S\chi\Theta\right)\overset{\circ}{\widetilde{\rho}}(1) + \left(\overline{\kappa}S+(1-\chi\Theta)+\overline{\kappa}_p-\overset{\circ}{V}\right)\overset{\circ}{\rho}(0), \\ A_4^1 = & \Theta\overline{\kappa}(1+S)\left(\overline{\beta}-3\overline{\alpha}\right), \\ A_1^2 = & -\overline{\nu}, \quad A_2^2 = -\overline{\kappa}\chi\Theta-\overline{\kappa}_p, \quad A_2^{2'} = \overline{\kappa}(1+\chi\Theta)+\overline{\kappa}_p+\overset{\circ}{V}, \\ A_3^2 = & \overline{\kappa}S(1-\chi\Theta)+\overline{\kappa}_p-\overset{\circ}{V}, \quad A_3^{2'} = \overline{\kappa}S\chi\Theta-\overline{\kappa}_p, \\ A_4^2 = & \Theta\overline{\kappa}\left(\chi\Theta(1+S)-S\right), \quad A_4^{2'} = -\Theta\overline{\kappa}\left(\chi\Theta(1+S)+1\right) \end{cases} \tag{A.2}$$

The linear operator $\mathscr{B}$ also introduced in (7) is defined by

$$\mathscr{B}\begin{pmatrix}\\ \partial_t\mathbf{q}_n,\partial_t\mathbf{q}_{n+1}\\ \\ \end{pmatrix} := \begin{pmatrix} (u-1)\overset{\circ}{\widetilde{\rho}}'(u)\delta\dot{x}_n - u\overset{\circ}{\widetilde{\rho}}'(u)\delta\dot{x}_{n+1} \\ \overset{\circ}{\widetilde{\rho}}(1)\delta\dot{x}_{n+1} \\ \overset{\circ}{\widetilde{\rho}}(0)\delta\dot{x}_n \\ \delta\dot{x}_n \end{pmatrix} + \begin{pmatrix} \partial_t\delta\widetilde{\rho}_n(u,t) \\ 0 \\ 0 \\ 0 \end{pmatrix}. \tag{A.3}$$

Expressions of the operators $\widehat{\mathscr{A}}_k$ and $\widehat{\mathscr{B}}_k$

As explained in Section 2.2, these operators are obtained by inserting (8) in (7). The operator $\widehat{\mathscr{A}}_k$ reads

$$\widehat{\mathscr{A}}_k\widehat{\mathbf{q}} = \begin{pmatrix} \widehat{A}_1^1(u)\delta\widehat{x} \\ \widehat{A}_2^1\delta\widehat{x} \\ \widehat{A}_3^1\delta\widehat{x} \\ \widehat{A}_4^1\delta\widehat{x} \end{pmatrix} + \begin{pmatrix} \widehat{A}_1^2\,\delta\widehat{\rho}(u) \\ \widehat{A}_2^2\,\delta\widehat{\rho}(0) + \widehat{A}_2^{2'}\,\delta\widehat{\rho}(1) \\ \widehat{A}_3^2\,\delta\widehat{\rho}(0) + \widehat{A}_3^{2'}\,\delta\widehat{\rho}(1) \\ \widehat{A}_4^2\,\delta\widehat{\rho}(0) + \widehat{A}_4^{2'}\,\delta\widehat{\rho}(1) \end{pmatrix} + \begin{pmatrix} \widehat{A}_1^3\,\delta\widehat{\rho}'(u) \\ \widehat{A}_2^3\,\delta\widehat{\rho}'(1) \\ \widehat{A}_3^3\,\delta\widehat{\rho}'(0) \\ 0 \end{pmatrix} + \begin{pmatrix} \widehat{A}_1^4\,\delta\widehat{\rho}''(u) \\ 0 \\ 0 \\ 0 \end{pmatrix}, \tag{A.4}$$

where

$$\begin{cases}
\widehat{A}_1^1(u) = & (-1+\mathrm{e}^{ik})\Big(2\overline{F} - 2\overline{\nu}\widehat{\rho}^{\mathrm{o}}(u) + \overset{\mathrm{o}}{V}\widehat{\rho}^{\mathrm{o}\prime}(u)\Big), \\
\widehat{A}_2^1 = & (-1+\mathrm{e}^{ik})\Big(\overline{\kappa}\Big(\big(\mathrm{e}^{ik}-1\big)\Big(3\overline{\alpha}-\overline{\beta}\Big) + (\widehat{\rho}^{\mathrm{o}}(1)-\widehat{\rho}^{\mathrm{o}}(0))\chi\Theta + \widehat{\rho}^{\mathrm{o}}(1) - 1\Big) \\
& \qquad + \widehat{\rho}^{\mathrm{o}}(1)\Big(\overline{\kappa}_p + \overset{\mathrm{o}}{V}\Big) - \overline{\kappa}_p\widehat{\rho}^{\mathrm{o}}(0)\Big), \\
\widehat{A}_3^1 = & (-1+\mathrm{e}^{ik})\Big(\overline{\kappa}S\Big(\big(1-\mathrm{e}^{-ik}\big)\Big(3\overline{\alpha}-\overline{\beta}\Big) - \widehat{\rho}^{\mathrm{o}}(0)(\chi\Theta-1) + \widehat{\rho}^{\mathrm{o}}(1)\chi\Theta - 1\Big) \\
& \qquad + \widehat{\rho}^{\mathrm{o}}(0)\Big(\overline{\kappa}_p - \overset{\mathrm{o}}{V}\Big) - \overline{\kappa}_p\widehat{\rho}^{\mathrm{o}}(1)\Big), \\
\widehat{A}_4^1 = & -2\overline{\kappa}(S+1)\chi\Theta\Big(3\overline{\alpha}-\overline{\beta}\Big)(\cos(k)-1), \\
\widehat{A}_1^2 = & -\overline{\nu}, \quad \widehat{A}_2^2 = -\mathrm{e}^{ik}\Big(\overline{\kappa}\chi\Theta + \overline{\kappa}_p\Big), \quad \widehat{A}_2^{2\prime} = \overline{\kappa} + \overline{\kappa}_p + \overline{\kappa}\chi\Theta + \overset{\mathrm{o}}{V}, \\
\widehat{A}_3^2 = & -\overline{\kappa}S\chi\Theta + \overline{\kappa}S + \overline{\kappa}_p - \overset{\mathrm{o}}{V}, \quad \widehat{A}_3^{2\prime} = \mathrm{e}^{-ik}\Big(\overline{\kappa}S\chi\Theta - \overline{\kappa}_p\Big), \\
\widehat{A}_4^2 = & \overline{\kappa}\Theta\Big((S+1)\chi\Theta - S\Big), \quad \widehat{A}_4^{2\prime} = -\mathrm{e}^{-ik}\overline{\kappa}\Theta\Big((S+1)\chi\Theta + 1\Big), \\
\widehat{A}_1^3 = & \overset{\mathrm{o}}{V}, \quad \widehat{A}_2^3 = 1, \quad \widehat{A}_3^3 = -1, \quad \widehat{A}_1^4 = 1,
\end{cases} \tag{A.5}$$

and the terms in red derive from dynamics (see Section 5). The corresponding expression for the operator $\widehat{\mathscr{B}}_k$ is

$$\widehat{\mathscr{B}}_k\widehat{\mathbf{q}} = \begin{pmatrix} \widehat{B}_1^1(u)\delta\widehat{x} \\ \widehat{B}_2^1\delta\widehat{x} \\ \widehat{B}_3^1\delta\widehat{x} \\ \widehat{B}_4^1\delta\widehat{x} \end{pmatrix} + \begin{pmatrix} \widehat{B}_1^2\delta\widehat{\rho}(u) \\ 0 \\ 0 \\ 0 \end{pmatrix}, \tag{A.6}$$

with

$$\begin{cases}
\widehat{B}_1^1(u) = & -(1+(-1+\mathrm{e}^{ik})u)\widehat{\rho}^{\mathrm{o}\prime}(u), \quad \widehat{B}_2^1 = -\mathrm{e}^{ik}\widehat{\rho}^{\mathrm{o}}(1), \\
\widehat{B}_3^1 = & \widehat{\rho}^{\mathrm{o}}(0), \quad \widehat{B}_4^1 = -1, \quad \widehat{B}_1^2 = 1,
\end{cases} \tag{A.7}$$

with the terms in red also deriving from dynamics.

Appendix B. Numerical method

The eigenvalue problem (9) involves two operators $\widehat{\mathscr{A}}_k$ and $\widehat{\mathscr{B}}_k$ acting on the scalar variable $\delta\widehat{x}$ and on the function $\delta\widehat{\rho} : [0,1] \to \mathbb{C}$ and its derivatives. This problem is solved numerically using the Chebyshev collocation method [26], a pseudo-spectral method adapted to nonperiodic problems.

Consider a complex-valued function $f : u \in [0,1] \mapsto f(u) \in \mathbb{C}$ and let f_N be its Chebyshev series approximation truncated at order N,

$$f_N(u) := \sum_{n=0}^{N} \check{f}_n \check{T}_n(u), \tag{B.1}$$

where $\check{f}_n$ are the Chebyshev coefficients and $\check{T}_n$ denote the Chebyshev polynomials of the first kind,[5] depicted in Fig. B.10 for $n = 0\ldots5$, and defined on [0,1] by the recurrence relationship

$$\check{T}_0(u) = 1, \quad \check{T}_1(u) = 2u-1, \quad \check{T}_n = (4u-2)\check{T}_{n-1} - \check{T}_{n-2} = 0 \quad \text{for } n \geq 2. \tag{B.2}$$

To compute the Chebyshev coefficients $\check{f}_n$, we use the collocation method on the Gauss-Lobato points $u_0, \ldots, u_N$ defined as

[5] The Chebyshev polynomials of the first kind $\check{T}_n$ defined on [0,1] used here are obtained by rescaling their traditional counterparts T_n defined on $[-1,1]$ via $\check{T}_n(u) := T_n(2u-1),\ \forall u \in [0,1]$.

$$u_n := \frac{1}{2}\left[\cos\left(\frac{\pi(N-n)}{N}\right)+1\right], \quad 0 \le n \le N, \tag{B.3}$$

and shown on Fig. B.10 for $N = 5$.

With the Chebyshev approximation, the first and second nderivatives of f are approximated by

$$f_N^{'}(u) = \sum_{n=0}^{N} \check{f}_n \check{T}_n^{'}(u), \quad f_N^{''}(u) = \sum_{n=0}^{N} \check{f}_n \check{T}_n^{''}(u). \tag{B.4}$$

The advantage of using the collocation method to compute the Chebyshev coefficients $\check{f}_n$ stems from the fact that the values of $f_N^{'}$ and $f_N^{''}$ at the collocation points u_n can be obtained using a fixed differentiation matrix $\check{\mathbf{D}}$ operating on the values of the function on the Gauss-Lobatto points $f_N(u_j)$:[6]

$$f_N^{'}(u_n) = \sum_{j=0}^{N} \check{D}_{nj} f_N(u_j). \tag{B.5}$$

Note that, with the Chebyshev method, the derivative at one point does not only depend on the neighboring points but on all the points of the domain which makes $\check{\mathbf{D}}$ a full matrix. Similarly, the second-order derivative is approximated using $(\check{\mathbf{D}})^2$.

To derive the discrete form of (9), each of the two operators $\widehat{\mathscr{A}}_k$ and $\widehat{\mathscr{B}}_k$ is decomposed as a sum of operators acting separately on $\delta\widehat{x}$, and $\delta\widehat{\rho}$ and its derivatives:

$$\widehat{\mathscr{A}}_k(\delta\widehat{x},\delta\widehat{\rho}) = \widehat{\mathscr{A}}_k^1\delta\widehat{x} + \widehat{\mathscr{A}}_k^2\delta\widehat{\rho} + \widehat{\mathscr{A}}_k^3\delta\widehat{\rho}^{'} + \widehat{\mathscr{A}}_k^4\delta\widehat{\rho}^{''}, \quad \widehat{\mathscr{B}}_k(\delta\widehat{x},\delta\widehat{\rho}) = \widehat{\mathscr{B}}_k^1\delta\widehat{x} + \widehat{\mathscr{B}}_k^2\delta\widehat{\rho}, \tag{B.6}$$

where the full expressions of the $\widehat{\mathscr{A}}_k^p$, $p = 1\ldots4$ and $\widehat{\mathscr{B}}_k^m$, $m = 1,2$ are given in Appendix A.

Using the decomposition (B.6), the operators $\widehat{\mathscr{A}}_k$ and $\widehat{\mathscr{B}}_k$ are approximated using the $(N+2)\times(N+2)$ matrices $\check{\mathbf{A}}_k$ and $\check{\mathbf{B}}_k$

$$\check{\mathbf{A}}_k\check{\mathbf{q}} = \check{\mathbf{A}}_k^1\delta\widehat{x} + \check{\mathbf{A}}_k^2\delta\check{\boldsymbol{\rho}} + \check{\mathbf{A}}_k^3\check{\mathbf{D}}\delta\check{\boldsymbol{\rho}} + \check{\mathbf{A}}_k^4\left(\check{\mathbf{D}}\right)^2\delta\check{\boldsymbol{\rho}}, \quad \check{\mathbf{B}}_k\check{\mathbf{q}} = \check{\mathbf{B}}_k^1\delta\widehat{x} + \check{\mathbf{B}}_k^2\delta\check{\boldsymbol{\rho}}, \tag{B.7}$$

where $\delta\check{\boldsymbol{\rho}} = (\delta\widehat{\rho}(u_0),\ldots,\delta\widehat{\rho}(u_N))$, $\check{\mathbf{q}} = (\delta\widehat{x},\delta\check{\boldsymbol{\rho}})$ and $\check{\mathbf{A}}_k^p$ $(p = 1,\ldots,4)$ and $\check{\mathbf{B}}_k^m$ $(m = 1,2)$ are the discretizations of the corresponding operators $\widehat{\mathscr{A}}_k^p$ and $\widehat{\mathscr{B}}_k^m$ on the Gauss-Lobatto mesh $\{u_i, 0 \le i \le N\}$.

This allows to discretize (9) into the following $(N+2)\times(N+2)$ generalized eigenvalue problem: For a given $k \in [0,\pi]$, find $(\lambda,\check{\mathbf{q}}) \in (\mathbb{C}\times\mathbb{C}^{N+2})$ with $\check{\mathbf{q}} \neq \mathbf{0}$ such that

$$\check{\mathbf{A}}_k\check{\mathbf{q}} = \lambda\check{\mathbf{B}}_k\check{\mathbf{q}}. \tag{B.8}$$

After solving (B.8) numerically, we consider the leading eigenvalue λ (the eigenvalue with the largest real part), which corresponds to the most critical growth rate.

As $\check{\mathbf{B}}_k$ is not invertible, (B.8) has less than $N+2$ eigenvalues. Indeed as can be deduced from (A.6) in Appendix A, the last three rows of $\check{\mathbf{B}}_k$ being linearly dependent, its kernel is of dimension 2. As a result, and noting that $\check{\mathbf{A}}^k$ is invertible, (B.8) has only N eigenvalues.

Convergence

We evaluate the convergence of the numerical method by considering the leading eigenvalue, and determine a satisfactory number of discretization points $N+1$.

For a given set of parameters ($\overline{F} = 10^{-2}, \overline{\nu} = 0, S = 1, \overline{\kappa} = 10, \overline{\kappa}_p = 0, \Theta = 0.01, \overline{\alpha} = 0, \overline{\beta} = 0$, and $k = \pi/2$), the leading eigenvalue with $N = 50$ is $-1.1271\cdot10^{-7} + 1.0000\cdot10^{-4}i$. Because of the spectral convergence properties of Chebyshev methods [26], full convergence with five significant digits of the leading eigenvalue is achieved with N as low as 5. This fast convergence has been verified for various sets of parameters, and we select the value $N = 10$ for the present analysis.

A superposition of eigenvalue spectra for different values of N is shown in Fig. B.11.

On top of the leading eigenvalue discussed above, we observe the progressive formation of two branches of constant imaginary part in the stable spectral plane. Note that, although these branches are not of particular interest for the linear stability analysis, and as expected from a consistent numerical method, they get more and more resolved as N increases.

[6] The coefficients of the $\check{\mathbf{D}}$ are obtained by adapting the differentiation matrix $\mathbf{D}$ found in Peyret [26], which corresponds to Chebyshev polynomials defined on $[-1,1]$, to the Chebyshev method reformulated on [0,1].

Appendix C. Material parameters of crystal growth

Based on the material properties of GaAs and Si found in the experimental literature, we select here the values of the dimensionless parameters of the step-flow problem (1). When no measured values of these parameters are available, we provide physically plausible ranges.

Upper bounds on the deposition and sublimation rates

Before referring to experimental works, we first note that the satisfaction of the "near equilibrium" assumption underlying the derivation of (1) (see Section 2.1 of Part I), which can be written in dimensional form as $|\rho_n(x,t) - \rho^*_{eq}| \ll \rho^*_{eq}$, imposes upper bounds on $\overline{F}$ and $\overline{\nu}$. Physically, given the finite diffusion speed of adatoms, a high deposition/evaporation rate may lead to terrace adatom densities that violate the "near equilibrium" assumption.

To estimate these bounds, consider first a train of equidistant steps in the deposition regime ($\overline{\nu} = 0$), under the assumption of infinite a/d velocities ($\overline{\kappa} \to \infty$). This simplifying assumption, which tends to underestimate the terrace adatom density, implies that $\overset{\circ}{\rho}{}^{\pm} = 1$ and $\widehat{\rho}^{\circ}(x) = 1 - \overline{F}x(x-1)/2$, with the maximal adatom density $\overset{\circ}{\rho}_{\max} = 1 + \overline{F}/8$ occurring at $x = 1/2$. Hence, limiting adatom density variations to, say, one fourth of the equilibrium value, yields the restriction $\overline{F} < 2$. Applying a similar reasoning to the evaporation case ($\overline{F} = 0$) yields $\overline{\nu} < 2.5$.

Hence, compliance with the near equilibrium assumption requires, in order of magnitude, $\overline{F}$ and $\overline{\nu}$ not to be more than unity. This condition is related to (and, in fact, is more stringent than) the condition of sufficiently slow deposition/evaporation, $\overline{F}\Theta < 1$ or $\overline{\nu}\Theta < 1$, found in Krug [21] and Michely and Krug [24]), which ensures that the crystal grows in the step-flow regime, i.e., without island nucleation.

Estimation of the equilibrium adatom coverage

The equilibrium adatom coverages for GaAs(001) and Si(111) have been measured by different groups, using the same technique of rapid quenching of an equilibrium vicinal surface and observation of islands resulting from adatom crystallization.

For GaAs(001), Johnson et al. Johnson et al., 1996 [see also Johnson et al., 1997; Tersoff et al., 1997] measured the equilibrium adatom coverage under typical molecular beam epitaxy conditions and found values between $\Theta = 0.05$ and $\Theta = 0.2$ for temperatures ranging between 570°C and 600°C.

For Si(111), we could not find data on the adatom coverage in the low temperature regime (650°C to 850°C) where silicon exhibits 7 $\times$7 surface reconstruction, and hence assume a low value of $\Theta = 0.01$.

Kinetic attachment/detachment

The ratio of attachment/detachment (a/d) kinetics to surface diffusion kinetics, reflects an a/d limited (ADL) regime when $\overline{\kappa} \ll 1$ and a diffusion limited (DL) regime when $\overline{\kappa} \gg 1$. In general, given the indeterminacy of the kinetic regime, we cover both regimes by considering values of $\overline{\kappa}$ ranging from 10^{-2} to 10^{2}.

More specifically, for Si(111)-7 $\times$ 7 it appears that the kinetic regime changes from ADL at low temperatures [between 400°C and 600°C, see Ichimiya et al., 1996] to DL at high temperature [around 860°C, see Hibino et al., 2001], however we have no direct information on the step kinetics in the temperature range 700°C − 800°C corresponding to the bunching experiments Omi et al., 2005 which we discuss in Section 4.1.

Ehrlich-Schwoebel effect

The Ehrlich–Schwoebel effect $S := \kappa_+/\kappa_-$, which quantifies the asymmetry of the a/d coefficients at the steps, is rarely clearly determined experimentally. In the absence of accurate information on the ES barrier, we explore here both the direct and the inverse ES effects, with a maximum ratio of the upper and lower attachment coefficients of an order of magnitude.

ES barrier in Si(111)-7 $\times$ 7

Measurements of the Ehrlich–Schwoebel effect for Si(111)-7 $\times$ 7 have been obtained using different means: comparison of the growth and decay rates of islands and holes Ichimiya et al., 1996; observation of denuded zones around steps Rogilo et al., 2013; Voigtlander et al., 1995 and of island nucleation distributions Chung and Altman, 2002. They lead to contradictory conclusions, i.e., a direct, negligible, or inverse ES effect. Consequently, we use the general range of $0.1 \le S \le 10$.

ES barrier in GaAs(001)

For GaAs(001), different studies yield values for the Ehrlich-Schwoebel barrier in reasonable agreement. By analyzing the characteristics of mounds during the epitaxial growth of GaAs, Šmilauer and Vvedensky [39] and Krug [20] derived values for the direct Schwoebel energy barrier of $\Delta E_- = 0.175$ eV and $\Delta E_- = 0.06$ eV, respectively. Krug [20] notes that his method underestimates—while that of Šmilauer and Vvedensky [39] overestimates—the value of the barrier so that these values should be considered as bounds. On the other hand, by performing atomistic computations that distinguish between two types of steps on the GaAs(001) surface (parallel and perpendicular to the arsenic dimers), Salmi et al. Salmi et al., 1999 obtain a value of the barrier of ΔE_-

$= 0.25$ eV for one type of step and conclude that there is no barrier for the second type of step.

We use here the intermediate value $\Delta E_- = 0.1$ eV, which, for the temperature of 600°C at which deposition is considered in Section 4, yields $S = \exp(\Delta E_-/k_B T) = 4$ [15]. In order to estimate the typical uncertainty, note that the parameters associated with the energetic barriers of Krug and Šmilauer and Vvedensky are $S = 2$ and $S = 10$, respectively.

Dipole-dipole elastic interaction coefficient $\overline{\alpha}$

Recall that the dimensionless elastic interaction coefficient is defined as $\overline{\alpha} = \alpha a^2/(k_B T L_0^3)$, where the dipole strength α is given by $\alpha = 4(1-\nu^2)(d_x^2 + d_z^2)/(\pi E)$. It depends on the strength of the dipole (d_x, d_z) representing the elastic field created by the steps during homoepitaxy.

Estimation of $\overline{\alpha}$ *in Si(111)-7* $\times$ *7*

This coefficient can be accurately estimated from the work of Stewart et al. [40]. Combining experimental measurements of the displacement field of a step with simulations, these authors determined the normal and tangential dipole moments: $d_z = 0.6$ eV/Å and $d_x = 1.5$ eV/Å. Given the effective isotropic elastic properties of silicon $E = 166$ GPa and $\nu = 0.2$ [40], we compute the elastic interaction coefficient $\alpha = 3$ eV.Å. For $T = 1000$ K and the reference terrace width $L_0 = 20$ nm, its dimensionless counterpart is estimated at $\overline{\alpha} = 5 \times 10^{-5}$. Since $\overline{\alpha} \propto L_0^{-3}$, if the initial terrace width is multiplied by two $\overline{\alpha}$ is decreased by an order of magnitude. Hence, $\overline{\alpha}$ may vary over several decades and elasticity may have a small or large effect on the stability depending on the initial miscut angle.

Estimation of $\overline{\alpha}$ *in GaAs(001)*

The interactions between steps along the GaAs(001) surface have recently been studied by Magri et al. Magri et al., 2014, Magri et al., 2016], using *ab initio* (density functional theory) computations. Through fitting of the atomic displacement field, they derived elastic dipole moments of the order of 0.1 eV/Å and a resulting elastic interaction coefficient of about $\alpha = 0.2$ eV.Å, with the exact value depending on the structure of each step. For an initial terrace width $L_0 = 16$ nm (which for a step height 0.28 nm corresponds to a miscut angle of 1°) and $T = 1000$ K, this yields $\overline{\alpha} = 5 \times 10^{-6}$.

References

[1] Benoit-Maréchal, L., Guin, L., Jabbour, M., Triantafyllidis, N., 2021. In preparation.

[2] Benoit-Maréchal, L., Jabbour, M., Triantafyllidis, N., 2021. Scaling laws for step bunching on vicinal surfaces: the role of the dynamical and chemical effects. Submitted, arXiv:2104.13830.

Chung, W.F., Altman, M.S., 2002. Kinetic length, step permeability, and kinetic coefficient asymmetry on the Si(111) (7x7) surface. Physical Review B 66 (7). https://doi.org/10.1103/physrevb.66.075338.

[4] Dufay, M., Frisch, T., Debierre, J.-M., 2007. Role of step-flow advection during electromigration-induced step bunching. Physical Review B 75 (24). https://doi.org/10.1103/physrevb.75.241304.

[5] Fanion, T., Fernández, M., Tallec, P.L., 2000. Deriving adequate formulations for fluid-structure interaction problems: from ALE to transpiration. Revue Européenne des Éléments Finis 9 (6–7), 681–708. https://doi.org/10.1080/12506559.2000.10511481.

[6] Ghez, R., Cohen, H.G., Keller, J.B., 1990. Stability of crystals that grow or evaporate by step propagation. Appl Phys Lett 56 (20), 1977–1979. https://doi.org/10.1063/1.103016.

[7] Ghez, R., Cohen, H.G., Keller, J.B., 1993. The stability of growing or evaporating crystals. J Appl Phys 73 (8), 3685–3693. https://doi.org/10.1063/1.352928.

[8] Gillet, F., 2000. Dynamique non linéaire de surfaces vicinales hors de équilibre. Université Joseph Fourier, Grenoble, France. https://www.theses.fr/2000GRE10204.

[9] Guin, L., Jabbour, M., Shaabani-Ardali, L., Benoit-Maréchal, L., Triantafyllidis, N., 2020. Stability of vicinal surfaces: beyond the quasistatic approximation. Phys. Rev. Lett. 124 (3) https://doi.org/10.1103/physrevlett.124.036101.

[10] Hata, K., Kawazu, A., Okano, T., Ueda, T., Akiyama, M., 1993. Observation of step bunching on vicinal gaas(100) studied by scanning tunneling microscopy. Appl Phys Lett 63 (12), 1625–1627. https://doi.org/10.1063/1.110716.

Hibino, H., Hu, C.-W., Ogino, T., Tsong, I.S.T., 2001. Decay kinetics of two-dimensional islands and holes on Si(111) studied by low-energy electron microscopy. Physical Review B 63 (24). https://doi.org/10.1103/physrevb.63.245402.

Ichimiya, A., Tanaka, Y., Ishiyama, K., 1996. Quantitative measurements of thermal relaxation of isolated silicon hillocks and craters on the Si(111)-(7x7) surface by scanning tunneling microscopy. Phys. Rev. Lett. 76 (25), 4721–4724. https://doi.org/10.1103/physrevlett.76.4721.

Ishizaki, J., Goto, S., Kishida, M., Fukui, T., Hasegawa, H., 1994. Mechanism of multiatomic step formation during metalorganic chemical vapor deposition growth of GaAs on (001) vicinal surface studied by atomic force microscopy. Jpn J Appl Phys 33 (1S), 721. https://doi.org/10.1143/JJAP.33.721.

Ishizaki, J., Ohkuri, K., Fukui, T., 1996. Simulation and observation of the step bunching process grown on GaAs(001) vicinal surface by metalorganic vapor phase epitaxy. Jpn J Appl Phys 35 (2S), 1280. https://doi.org/10.1143/JJAP.35.1280.

[15] Jeong, H.-C., Williams, E.D., 1999. Steps on surfaces: experiment and theory. Surf Sci Rep 34 (6), 171–294. https://doi.org/10.1016/S0167-5729(98)00010-7.

Johnson, M., Leung, K., Birch, A., Orr, B., 1997. Adatom concentration on GaAs(001) during annealing. J Cryst Growth 174 (1), 572–578. https://doi.org/10.1016/S0022-0248(97)00039-0.

Johnson, M., Leung, K., Birch, A., Orr, B., Tersoff, J., 1996. Adatom concentration on GaAs(001) during MBE annealing. Surf Sci 350 (1), 254–258. https://doi.org/10.1016/0039-6028(95)01110-2.

Kasu, M., Fukui, T., 1992. Multi-atomic steps on metalorganic chemical vapor deposition-grown GaAs vicinal surfaces studied by atomic force microscopy. Jpn J Appl Phys 31 (7A), L864. https://doi.org/10.1143/JJAP.31.L864.

[19] Keller, J.B., Cohen, H.G., Merchant, G.J., 1993. The stability of rapidly growing or evaporating crystals. J Appl Phys 73 (8), 3694–3697. https://doi.org/10.1063/1.352929.

[20] Krug, J., 1997. Origins of scale invariance in growth processes. Adv Phys 46 (2), 139–282. https://doi.org/10.1080/00018739700101498.

[21] Krug, J., 2005. Introduction to step dynamics and step instabilities. In: Voigt, A. (Ed.), Multiscale Modeling in Epitaxial Growth. Birkhäuser Basel, Basel, pp. 69–95. https://doi.org/10.1007/3-7643-7343-1_6.

Magri, R., Gupta, S.K., Rosini, M., 2014. Step energy and step interactions on the reconstructed GaAs(001) surface. Physical Review B 90 (11). https://doi.org/10.1103/physrevb.90.115314.

Magri, R., Gupta, S.K., Rosini, M., 2016. Erratum: step energy and step interactions on the reconstructed GaAs(001) surface [phys. rev. b 90, 115314 (2014)]. Physical Review B 94 (23). https://doi.org/10.1103/physrevb.94.239909.

[24] Michely, T., Krug, J., 2012. Islands, mounds and atoms, 42. Springer Science & Business Media. https://doi.org/10.1007/978-3-642-18672-1.
Omi, H., Homma, Y., Tonchev, V., Pimpinelli, A., 2005. New types of unstable step-flow growth on Si(111)-(7x7) during molecular beam epitaxy: scaling and universality. Phys. Rev. Lett. 95 (21) https://doi.org/10.1103/physrevlett.95.216101.
[26] Peyret, R., 2002. Spectral methods for incompressible viscous flow, 148. Springer-Verlag. https://doi.org/10.1007/978-1-4757-6557-1.
[27] Pierre-Louis, O., 2003. Step bunching with general step kinetics: stability analysis and macroscopic models. Surf Sci 529 (1), 114–134. https://doi.org/10.1016/S0039-6028(03)00075-X.
[28] Pimpinelli, A., Videcoq, A., 2000. Novel mechanism for the onset of morphological instabilities during chemical vapour epitaxial growth. Surf Sci 445 (1), L23–L28. https://doi.org/10.1016/s0039-6028(99)01100-0.
[29] Politi, P., Krug, J., 2000. Crystal symmetry, step-edge diffusion, and unstable growth. Surf Sci 446 (1–2), 89–97. https://doi.org/10.1016/s0039-6028(99)01104-8.
Pond, K., 1994. Step bunching and step equalization on vicinal GaAs(001) surfaces. Journal of Vacuum Science & Technology B: Microelectronics and Nanometer Structures 12 (4), 2689. https://doi.org/10.1116/1.587232.
[31] Ranguelov, B., Muller, P., Metois, J.-J., Stoyanov, S., 2017. Step density waves on growing vicinal crystal surfaces – theory and experiment. J Cryst Growth 457, 184–187. https://doi.org/10.1016/j.jcrysgro.2016.06.041.
[32] Ranguelov, B., Stoyanov, S., 2007. Evaporation and growth of crystals: propagation of step-density compression waves at vicinal surfaces. Physical Review B 76 (3). https://doi.org/10.1103/physrevb.76.035443.
[33] Ranguelov, B., Stoyanov, S., 2008. Instabilities at vicinal crystal surfaces: competition between electromigration of adatoms and kinetic memory effect. Physical Review B 77 (20). https://doi.org/10.1103/physrevb.77.205406.
Rogilo, D.I., Fedina, L.I., Kosolobov, S.S., Ranguelov, B.S., Latyshev, A.V., 2013. Critical terrace width for two-dimensional nucleation during si growth on Si(111)-(7x7) surface. Phys. Rev. Lett. 111 (3) https://doi.org/10.1103/physrevlett.111.036105.
Salmi, M., Alatalo, M., Ala-Nissila, T., Nieminen, R., 1999. Energetics and diffusion paths of gallium and arsenic adatoms on flat and stepped GaAs(001) surfaces. Surf Sci 425 (1), 31–47. https://doi.org/10.1016/s0039-6028(99)00180-6.
[36] Sekerka, R., 1967. Application of the time-dependent theory of interface stability to an isothermal phase transformation. J. Phys. Chem. Solids 28 (6), 983–994. https://doi.org/10.1016/0022-3697(67)90215-6.
Shinohara, M., Inoue, N., 1995. Behavior and mechanism of step bunching during metalorganic vapor phase epitaxy of GaAs. Appl Phys Lett 66 (15), 1936–1938. https://doi.org/10.1063/1.113282.
[38] Slanina, F., Krug, J., Kotrla, M., 2005. Kinetics of step bunching during growth: a minimal model. Physical Review E 71 (4). https://doi.org/10.1103/physreve.71.041605.
[39] Šmilauer, P., Vvedensky, D.D., 1995. Coarsening and slope evolution during unstable spitaxial growth. Physical Review B 52 (19), 14263–14272. https://doi.org/10.1103/physrevb.52.14263.
[40] Stewart, J., Pohland, O., Gibson, J.M., 1994. Elastic-displacement field of an isolated surface step. Phys. Rev. B 49, 13848–13858. https://doi.org/10.1103/PhysRevB.49.13848.
Tejedor, P., Allegretti, F., Šmilauer, P., Joyce, B., 1998. Temperature-dependent unstable homoepitaxy on vicinal GaAs(110) surfaces. Surf Sci 407 (1–3), 82–89. https://doi.org/10.1016/s0039-6028(98)00149-6.
Tersoff, J., Johnson, M.D., Orr, B.G., 1997. Adatom densities on GaAs: evidence for near-equilibrium growth. Phys. Rev. Lett. 78, 282–285. https://doi.org/10.1103/PhysRevLett.78.282.
[43] Vladimirova, M., Vita, A.D., Pimpinelli, A., 2001. Dimer diffusion as a driving mechanism of the step bunching instability during homoepitaxial growth. Physical Review B 64 (24). https://doi.org/10.1103/physrevb.64.245420.
[44] Voigtlander, B., Zinner, A., Weber, T., Bonzel, H.P., 1995. Modification of growth kinetics in surfactant-mediated epitaxy. Physical Review B 51 (12), 7583–7591. https://doi.org/10.1103/physrevb.51.7583.